Technobius

A peer-reviewed open-access journal

Contacts:
Website: https://technobius.kz/
E-mail: technobius.research@gmail.com

CONTENTS

Article

Utilization of water treatment plant sludge in concrete mix

Kairat Ospanov[1,*], Dariusz Andraka[2], Manat Alzhigitova[1], Bakhtiyar Kabylbekov[1], Gulbanu Mukhanova[3]

[1]Department of Hydrogeology, Institute of Geology and Oil-Gas Business, Satbayev University, Almaty, Kazakhstan
[2]Department of Water Supply and Sewage Systems, Faculty of Civil Engineering and Environmental Sciences, Bialystok University of Technology, Bialystok, Poland
[3]State Municipal Enterprise «Almaty Su», Almaty, Kazakhstan
*Correspondence: k.ospanov@satbayev.university

Abstract. This article presents the results of research on the processing of sludge generated at the Main Treatment Facilities (MTF) of Almaty, Kazakhstan, for use in concrete mixes. A nominal concrete mix composition was selected for sample production, consisting of Portland cement, crushed stone, sand, water, Interplast AT superplasticizer, and sludge from the horizontal settling tanks of the MTF. Samples were tested for compressive and flexural strength, water absorption, permeability, and density, revealing that replacing 5% sand with MTF sludge decreases compressive and flexural strengths at 28 days by 13.3% and 3.7%, respectively. In terms of water absorption, the best performance was observed in the sample containing 10% sludge from the MTF replacing part of the sand.
Keywords: water treatment, settling tank, water supply, sludge, paving slab, strength, water absorption, permeability.

1. Introduction

Water supply and wastewater services in Almaty are provided by the State Municipal Enterprise «Almaty Su». The city's water supply is from 4 main sources: the Bolshaya Almatinka and Malaya Almatinka rivers, as well as underground wells from the Almaty and Talgar aquifers. The total design capacity of these sources is 1.343 thousand m³/day. The water intake from the Bolshaya Almatinka River with its treatment facilities is a key source of Almaty's drinking water, meeting approximately 35% of the city's demand. The Main Water Treatment Facilities (MTF) are located in the southwest of Almaty, on the right bank of the Bolshaya Almatinka River, on a site with a slight slope from southwest to northeast. The maximum designed capacity of the MTF is 254 thousand m³/day [1]. The technological scheme of the Almaty MTF is shown in Figure 1 [2], [3].
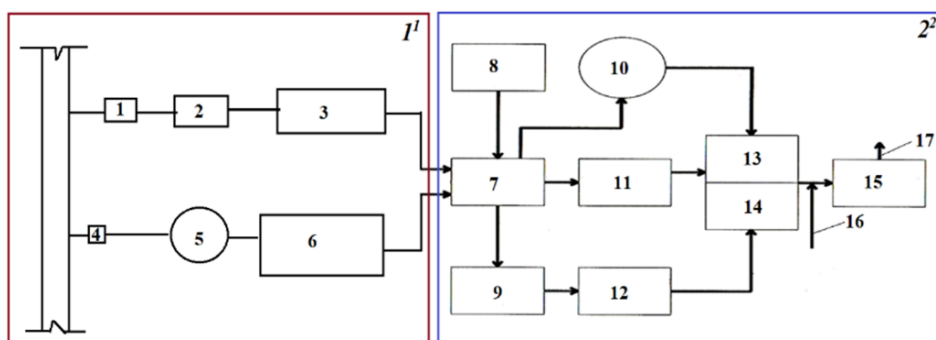
Figure 1 – Technological scheme of the MTF [2], [3]: 1[1] – Water intake structures; 2[2] – Water treatment facilities; 1 – Ice discharge; 2 – Sand trap; 3 – Daily regulation basin (DRB-1), 4 –

Venturi flume; 5 – Radial settling tank; 6 – Daily regulation basin (DRB-2); 7 – Distribution chamber; 8 – Reagent facility; 9 – Drum screens; 10 – Radial settlers with spiral guides; 11 – Vertical settlers; 12 – Horizontal settlers; 13 – Rapid filters (2nd stage); 14 – Rapid filters (3rd stage); 15 – Clear water reservoirs; 16 – Sodium hypochlorite dosing for disinfection; 17 – Water supply to consumers.

According to Figure 1, at the MTF, sludge is generated in radial settlers with spiral guides, in vertical settlers, and in horizontal settlers. Sludge removal from the settlers is performed using hydrostatic pressure to discharge it into the sewer system. Currently, sludge from the Almaty water treatment facilities is disposed of through the municipal sewer network, which then directs it to the wastewater treatment facilities. The problem of sludge utilization from water treatment facilities is of particular importance as it has both environmental and economic significance, contributing to the recovery of raw materials and resources. The level of sludge utilization in Kazakhstan remains low.

Sludge forms during clarification and sedimentation at various stages of water treatment and typically amounts to 1-3% of the volume of treated water. The main objectives of sludge treatment are to ensure environmental safety, reduce sludge volume to minimize landfill area requirements, and prepare sludge for reuse as secondary raw materials Depending on the water treatment technology, sludge may form in settling tanks, clarifiers with suspended sludge layers, during sedimentation of filter backwash water, contact clarifiers, and others [4], [5].

One of the most promising uses for water treatment sludge is in the production of construction materials [6]. Sludges containing clay fractions can be added to raw mixes for ceramic materials, improving plasticity, reducing firing temperature, or replacing part of the traditional clay components [7], [8].

An interesting approach involves producing alumina cement from natural water sludge [9]. Sludge can be used as an additive in cement production or as a component of concrete mixtures. Depending on its chemical composition, it may serve as a mineral additive, filler, or modifying component [9], [10]. Although not directly related to construction materials, it is worth mentioning that sludge rich in organic matter can be used to produce soil substrates for landscaping. Studies have shown that such substrates exhibit excellent anti-erosion properties [11]. Among all options, the utilization of water treatment sludge in construction materials and products appears to be the most promising. Processed sludge represents a key reserve of material and energy resources for the construction industry and related sectors. However, applying such sludge utilization methods in Kazakhstan requires further research, as these approaches may sometimes degrade the quality of the final products and may not always be environmentally sound. Therefore, there is a need to develop highly efficient technologies for the use of water treatment sludge in construction materials that consider Kazakhstan's specific natural and climatic conditions.

This study proposes using sludge from Almaty's water treatment facilities as an additive in concrete mixtures. Laboratory experimental research was conducted to determine the optimal sludge content in concrete mixtures.

2. Methods

To produce concrete mixtures containing sludge from the MTF, a nominal concrete mix was selected. The initial mix design (without additives) was calculated using the method described in [12]. This method is based on determining the total absolute volumes of materials needed to produce 1 m³ of concrete.

The primary components for producing concrete samples included Portland cement, crushed stone, sand, water, sludge from the horizontal settlers of the MTF, and the Interplast AT superplasticizer.

In the laboratory experiments, the binder used was Portland cement CEM II/A-K(S-I) 32.5N, M450, produced by the Zhambyl Cement Production Company, LLP (Taraz, Kazakhstan).

The Interplast AT superplasticizer manufactured by GOODHIM (Krasnoyarsk, Russia) was used as a plasticizing additive. The tap water per [13] was used for mixing. The superplasticizer was added together with the mixing water.

The fine aggregate was construction sand produced in Kazakhstan, with a particle size range of 1.3 mm to 3.5 mm. The coarse aggregate was crushed stone produced in Kazakhstan. Albite porphyry crushed stone with particle sizes ranging from 5 to 20 mm, free of clay lumps, was used. The crushed stone had a strength grade of M1400, wear resistance grade I1, no weak particles, and frost resistance grade F300. Its bulk density was 1430 kg/m³.

Sludge for the laboratory experiments was obtained from the horizontal settlers of the MTF by the State Municipal Enterprise «Almaty Su». Sampling was performed manually. After air drying, the sludge had a moisture content of 2.1%.

Concrete samples were produced according to the mix composition shown in Table 1.

Table 1 – Composition of the studied concrete mixes per 1 m^3

Mix No.	Cement, kg	Crushed Stone, kg	Sand, kg	Water, kg	Superplasticizer, l	Sludge from, kg
1 (design)	310	1219	661	180	-	-
2 (reference)	310	1219	661	180	3.72	-
3	310	1219	628	180	3.72	33
4	310	1219	595	180	3.72	66
5	310	1219	562	180	3.72	99

Some photographs of concrete samples and sludge from the MTF are shown in Figure 2.

Figure 2 – Photographs of concrete samples and sludge from the MTF

Sample testing was conducted using standard methods in the laboratories of Satbayev University (Almaty, Kazakhstan).

Flexural and compressive strength tests were performed on 100×100×400 mm and 100×100×100 mm samples following [14]. The water absorption of the concrete samples was measured to assess their suitability for use in paving slab production according to [15]. The water permeability of the concrete samples was determined next. Water permeability refers to the concrete's ability to resist water penetration under pressure, which is a key indicator of its quality and durability [16]. Several methods can be used to measure concrete water permeability, including

the "wet spot" method, filtration coefficient, "depth of water penetration," and "air permeability." The latter method and an AGAMA-2RM device were used in this study. Two sets of control samples, each containing eight cylindrical samples (form FC-150), were prepared. The samples were fully cured (28 days) under standard conditions (temperature 20 ± 2 °C, relative humidity 95 ± 5%) according to [17]. The density testing was conducted according to [18].

3. Results and Discussion

Figure 3 shows the results of compression tests.
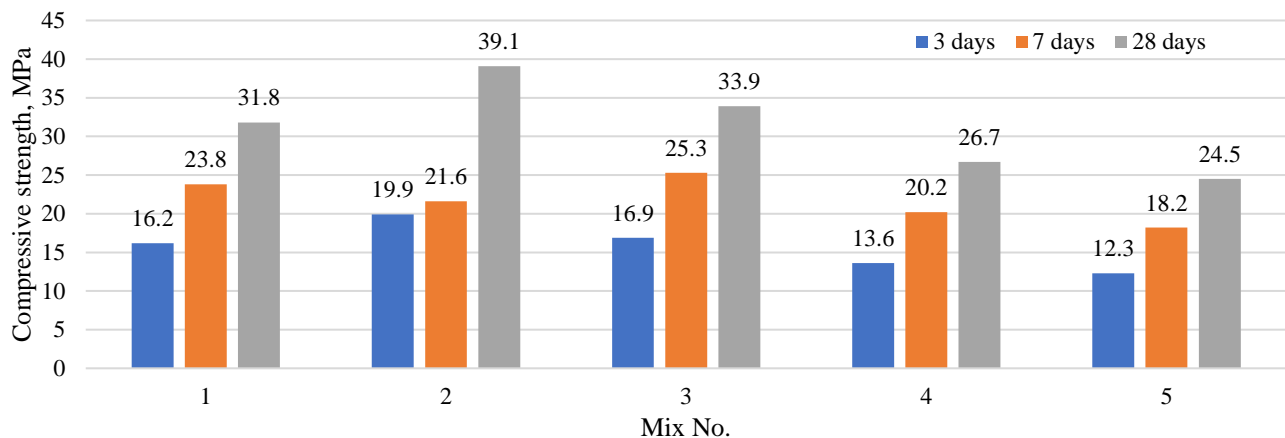
Figure 3 – Compressive strength of the samples

Analysis of the obtained results shows that the highest compressive strength at 28 days is achieved in mix No. 2, reaching 39.1 MPa. Mix No. 5, in turn, demonstrates the lowest strength at all stages: 12.3 MPa at 3 days, 18.2 MPa at 7 days, and 24.5 MPa at 28 days. These data may indicate low reactivity or a suboptimal composition of mix No. 5.

Figure 4 shows the results of the tests for the flexural strength.
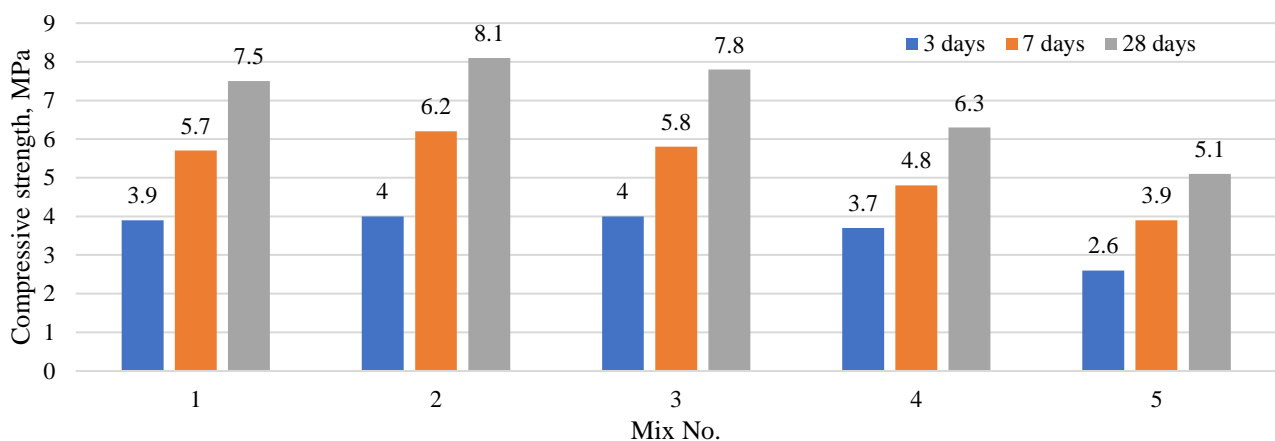
Figure 4 – Flexural strength of the samples

Analysis of the results shown in Figures 3 and 4 indicates that even with the introduction of 5% water supply sludge from the MTF to replace part of the sand, the strength characteristics of the concrete mix decrease. The achieved strength indicators suggest the potential for producing concrete paving slabs using the developed concrete mixes with the addition of up to 5% of water treatment plant sludge. Overall, the use of dewatered water supply sludge in concrete production is considered highly promising due to potential economic and environmental benefits.

Figure 5 shows the results of water absorption tests.
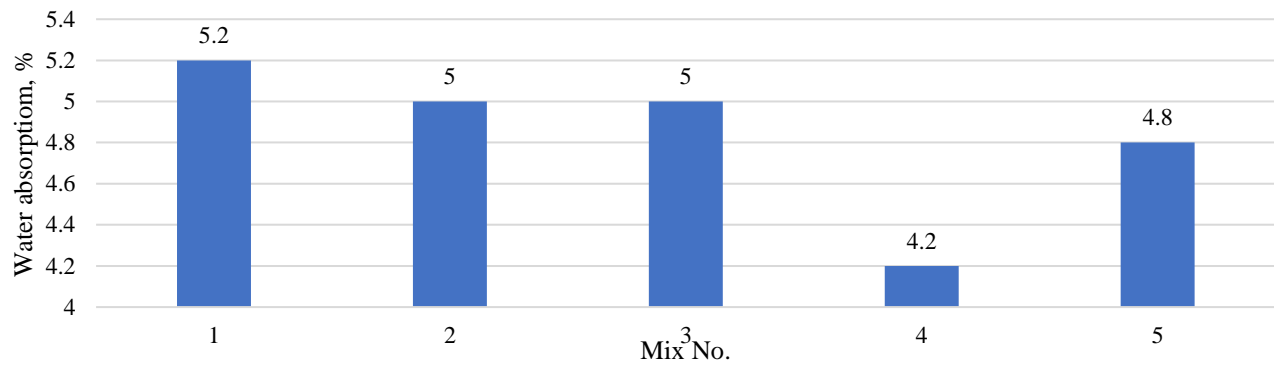
Figure 5 – Water absorption of samples

The results of laboratory tests of concrete samples for water absorption show significant variations depending on the mix composition. Mix No. 4, prepared with a sand-to-sludge ratio of 10%, exhibited the lowest water absorption at 4.2%. This indicates its denser structure compared to other mixes, which is a favorable factor for concrete durability. Conversely, mix No. 1 has the highest water absorption at 5.2%, which may indicate a more porous structure or a greater number of voids in the mix, potentially reducing its resistance to water and frost. In general, lower water absorption indicates a denser concrete structure and, consequently, better resistance to aggressive environmental impacts.

Table 2 shows the results of air permeability tests.

Table 2 – Permeability of the samples

Mix Number	Air permeability resistance of concrete samples (m), s/cm³	Air permeability parameter (a), cm³/s	Water permeability grade, W
1 (design)	6.2	0.161	W6
2 (reference)	6.4	0.156	W6
3	7.1	0.141	W6
4	9.6	0.104	W8
5	9.9	0.101	W8

Analysis of the air permeability data shows that mixes No. 4 and No. 5 demonstrate the best performance, achieving a rating of W8 due to their high resistance to air penetration. In contrast, mixes No. 1, No. 2, and No. 3 have a lower rating of W6, indicating a less dense structure and, consequently, lower water resistance. The increased resistance of the concrete to air penetration is attributed to the improved quality of the modified cement matrix and concrete structure due to the presence of MTF sludge and the Interplast AT superplasticizer.

Figure 6 shows the results of density tests.
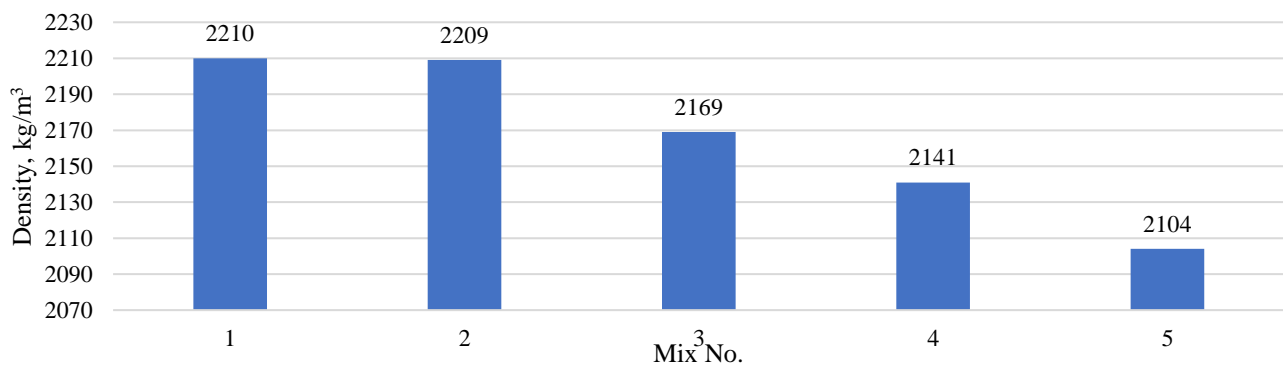
Figure 6 – Summary data on the density index

Analysis of the results in Figure 6 shows that mix No. 1 demonstrates the highest density (2220 kg/m³), slightly ahead of mix No. 2 (2210 kg/m³) and mix No. 3 (2209 kg/m³). Mixes No. 4

(2141 kg/m³) and No. 5 (2104 kg/m³) show lower density values, with mix No. 5 having the lowest density among all presented mixes. This indicates that replacing part of the sand with water supply sludge from the MTF results in a decrease in the density of concrete products.

4. Conclusions

Based on the results of laboratory experimental studies, it was established that the addition of the Interplast AT superplasticizer at a dosage of 1.2 liters per 100 kg of cement to concrete products leads to a significant increase in their strength: compressive strength at 28 days increases by 18.7%, and flexural tensile strength at 28 days increases by 7.4%.

It was also established that introducing 5% water supply sludge from the Main Treatment Facilities (MTF) of Almaty to replace part of the sand results in reduced strength characteristics of concrete products: compressive strength at 28 days decreases by 13.3%, and flexural tensile strength at 28 days decreases by 3.7%. The achieved strength indicators suggest the feasibility of producing concrete paving slabs using the developed concrete mixes with up to 5% sludge addition.

Laboratory test results for water absorption of concrete samples depending on the mix composition showed that the best performance was achieved with mix No. 4, prepared with a sand-to-sludge ratio of 10%. It was also found that replacing part of the sand with water supply sludge reduces the density of concrete products. Overall, the use of dewatered water supply sludge in concrete production is considered highly promising due to its potential economic and environmental benefits.

References

[1] Almaty Su, "Technological Regulations for the Operation of the Main Water Treatment Facilities on the Bolshaya Almatinka River in Almaty City," Almaty, 2015.

[2] K. Ospanov, Ye. Kuldeyev, U. Onglassyn, S. Merkuryeva, and G. Mukhanova, "Selecting a flocculant for treating sludge from wastewater treatment plants in Almaty," *Water, land and forest resources*, no. 4 (104), pp. 297–308, Dec. 2024, doi: 10.37884/4-2024/31.

[3] K. Ospanov, E. Kuldeyev, D. Andraka, and M. Alzhigitova, "Pilot Study on the Possibility of Improving Water Treatment Sludge Management in Almaty," *Water (Basel)*, vol. 16, no. 19, p. 2849, Oct. 2024, doi: 10.3390/w16192849.

[4] L. I. Qrenawi and F. K. J. Rabah, "Sludge management in water treatment plants: literature review," *Int J Environ Waste Manag*, vol. 27, no. 1, p. 93, 2021, doi: 10.1504/IJEWM.2021.111909.

[5] S. N. F. Zakaria, H. A. Aziz, Y.-T. Hung, M.-H. S. Wang, and L. K. Wang, "Treatment of Hazardous Sludge from Water and Wastewater Treatment Plants," in *Industrial Waste Engineering. Handbook of Environmental Engineering*, vol. 28, Cham: Springer, 2023, pp. 1–41. doi: 10.1007/978-3-031-46747-9_1.

[6] Z. He *et al.*, "Recycling drinking water treatment sludge in construction and building materials: A review," *Science of The Total Environment*, vol. 926, p. 171513, May 2024, doi: 10.1016/j.scitotenv.2024.171513.

[7] I. U. Aubakirova, "Use of sludge from water treatment plants in the production of building materials," *Water and Ecology*, vol. 25, no. 4, pp. 32–37, 2020, doi: 10.23968/2305-3488.2020.25.4.32-37.

[8] S. Ya. Davidov, R. A. Apakashev, and L. N. Oleynikova, "The variant of using precipitation water treatment for the production of building and ceramic materials," *NOVYE OGNEUPORY (NEW REFRACTORIES)*, no. 4, pp. 3–8, May 2023, doi: 10.17073/1683-4518-2023-4-3-8.

[9] T. M. S. Agra, V. M. E. Lima, P. E. A. Basto, and A. A. Melo Neto, "Characterizing and processing a kaolinite-rich water treatment sludge for use as high-reactivity pozzolan in cement manufacturing," *Appl Clay Sci*, vol. 236, p. 106870, May 2023, doi: 10.1016/j.clay.2023.106870.

[10] C. Y. Ching, M. J. K. Bashir, N. Choon Aun, and M. A. A. Aldahdooh, "Sustainable production of concrete with treated alum sludge," *Constr Build Mater*, vol. 282, p. 122703, May 2021, doi: 10.1016/j.conbuildmat.2021.122703.

[11] R. Aline, M. Edy Lenin Tejeda, and B. Maria Eugenia Gimenez, "Reuse of water treatment plant sludge mixed with lateritic soil in geotechnical works," *Environmental Challenges*, vol. 7, p. 100465, Apr. 2022, doi: 10.1016/j.envc.2022.100465.

[12] J. Dragomirová, M. Palou, K. Gméling, V. Szilágyi, I. Harsányi, and L. Szentmiklósi, "Experimental Study of Selected Properties of Heavyweight Concrete Based on Analysis of Chemical Composition and Radioactive Elements of its Components," *Solid State Phenomena*, vol. 321, pp. 113–118, Jul. 2021, doi: 10.4028/www.scientific.net/SSP.321.113.

[13] *GOST 23732-2011. Water for Concrete and Mortar. Technical Specifications*. Moscow, Russia, 2019, p. 18.

[14] *GOST 10180-2012. Concrete. Methods for Determining Strength Using Control Specimens*. Moscow, Russia, 2018, p. 36.

[15] *GOST 12730.3-2020. Concrete. Method for Determining Water Absorption*. Moscow, Russia, 2021, p. 14.

[16] T. K. Akchurin, V. D. Tukhareli, and O. Yu. Pushkarskaya, "The Modifying Additive for Concrete Compositions Based on the Oil Refinery Waste," *Procedia Eng*, vol. 150, pp. 1485–1490, 2016, doi: 10.1016/j.proeng.2016.07.087.

[17] *GOST 12730.5-2018. Concrete. Methods for Determining Water Permeability*. Moscow, Russia, 2019, p. 23.

[18] *GOST 12730.1-2020. Concrete. Method for Determining Density*. Moscow, Russia, 2021, p. 18.

Information about authors:

Kairat Ospanov – Candidate of Technical Sciences, Professor, Department of Hydrogeology, Institute of Geology and Oil-Gas Business, Satbayev University, Almaty, Kazakhstan, k.ospanov@satbayev.university

Dariusz Andraka – PhD, Professor, Department of Water Supply and Sewage Systems, Faculty of Civil Engineering and Environmental Sciences, Bialystok University of Technology, Bialystok, Poland, d.andraka@pb.edu.pl

Manat Alzhigitova – Senior Lecturer, Department of Hydrogeology, Institute of Geology and Oil-Gas Business, Satbayev University, Almaty, Kazakhstan, m.alzhigitova@satbayev.university

Bakhtiyar Kabylbekov – Master Student, Department of Hydrogeology, Institute of Geology and Oil-Gas Business, Satbayev University, Almaty, Kazakhstan, b12345r@mail.ru

Gulbanu Mukhanova – Head of Department, State Municipal Enterprise «Almaty Su», Almaty, Kazakhstan, gulbanu.mukhanova.67@mail.ru

Author Contributions:

Kairat Ospanov – concept, methodology, data collection, testing, modeling, analysis, interpretation, drafting, editing, funding acquisition.

Dariusz Andraka – concept, methodology, resources, data collection.

Manat Alzhigitova – data collection, testing, modeling, analysis, visualization, interpretation.

Bakhtiyar Kabylbekov – data collection, testing, modeling.

Gulbanu Mukhanova – resources, data collection, analysis, visualization, interpretation, editing.

Conflict of Interest: The authors declare no conflict of interest.

Use of Artificial Intelligence (AI): The authors declare that AI was not used.
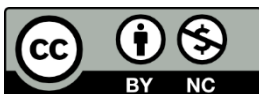
The influence of stabilizers on the strength characteristics of soils in the Western Kazakhstan region

Mariya Smagulova[1,2], Duman Dyussembinov[1], Jeong Ku Kang[3], Adiya Zhumagulova[1,2], Manarbek Zhumamuratov[2,*]

[1]Department of Technology of Industrial and Civil Engineering, L.N. Gumilyov Eurasian National University, Astana, Kazakhstan
[2]Scientific Research and Development Center, JSC "Kazakhstan Road Research Institute", Astana, Kazakhstan
[3]Department of Civil and Environmental Engineering, Incheon National University, Incheon, Republic of Korea.
*Correspondence: zhumamuratovmanarbek@gmail.com

Abstract. The paper presents the results of laboratory studies of soils in four regions of Western Kazakhstan: Atyrau, West Kazakhstan, Aktobe, and Mangystau regions. Laboratory tests determined their physical and mechanical properties, while IR Fourier spectroscopy was applied to analyze mineral composition. Modern stabilizing additives were introduced into the soils, and compressive strength was evaluated after 7 and 28 days. The results demonstrated a 1.5–2.5-fold increase in strength compared to untreated samples, with maximum values ranging from 4 to 6 MPa. The greatest effect was observed in sandy loams and carbonate-rich soils, confirming the high potential of stabilizers for enhancing road base performance in the region.
Keywords: road construction, soil stabilization, carbonate soils, IR Fourier spectroscopy, compressive strength.

1. Introduction

One of the pressing problems of road construction in the Western Kazakhstan region (WKR) is the low bearing capacity of local foundation soils. The climate of the region is characterized by sharp temperature fluctuations, dry summers, and cold winters, which, combined with the diversity of soil composition (sandy loam, clay loam) and their high sensitivity to moisture, lead to deformations and destruction of road surfaces [1].

The physical and mechanical properties of soils in road foundations depend primarily on their mineralogical composition, homogeneity, the presence of salts and organic residues, local climatic conditions, and hydrogeology, which have a significant impact on the stability of road infrastructure. Soil subsidence, its heaving, the presence of a soluble phase, filtration rate, and other characteristics of weak soils require study, taking into account the dynamic loads from large-capacity transport [2].

Being in a stressed state under the weight of the structure and its own weight, these soils, with an increase in humidity, provide additional subsidence deformation caused by a radical change in the soil structure [3]. In the current conditions, the development of moisture- and temperature-resistant road bases is one of the primary tasks [4].

In recent years, considerable attention has been paid to soil stabilization technologies as an effective method of improving the load-bearing capacity of problematic soils [5]. The use of mineral and chemical additives allows modifying soil structure, reducing water absorption, increasing strength and frost resistance, and thus extending the service life of road pavements. However, the effectiveness of such additives depends not only on their chemical composition, but also on the type of soil, climatic conditions, and methods of incorporation into the soil matrix [6].

Recent studies systematized various approaches to soil stabilization, showing that both mineral and polymer additives can significantly increase load-bearing capacity, but the degree of improvement strongly depends on soil type [7]. Some works demonstrated that biopolymers in combination with geosynthetics effectively increase cohesion and shear strength, although their efficiency decreases under higher cyclic stresses [8]. Other studies confirmed the potential of using local soils for road construction when treated with stabilizers, while highlighting the limitations imposed by salinity and mineralogical variability [9]. Investigations of geosynthetics proved their role in reducing subsidence and improving durability, but also revealed partial strength losses under long-term loading [10]. Overall, previous research emphasizes the need for approaches that directly relate mineralogical composition to mechanical performance after standard curing periods [11].

Therefore, the present study aims to conduct a comparative analysis of soils from four regions of Western Kazakhstan and to evaluate the effectiveness of modern stabilizers in relation to mineralogical composition determined by IR Fourier spectroscopy, with emphasis on compressive strength development and frost resistance.

2. Methods

The experimental study was aimed at determining the physical, mechanical, and structural properties of soils typical for WKR and evaluating the effectiveness of various stabilizing additives. The methodology included several stages of research.

First, the source materials were characterized in terms of granulometric composition, physical properties, and classification according to current national and interstate standards [12], [13], [14], [15]. The optimum moisture content and maximum density were established by standard laboratory procedures [16]. These characteristics provided the basis for selecting the preparation and compaction modes of the test specimens.

Next, the influence of inorganic binders on the properties of soils was assessed. For this purpose, mixtures of soils with Portland cement M400 and the following experimental stabilizers were prepared (Figure 1): 1) "EZCON" high concentration; 2) "EZCON" low concentration; 3) "ANT"; 4) "Gistrong pul"; 5) "Nova create"; 6) "Gistrong". Laboratory cylindrical samples with a diameter and height of 71.4 mm were molded at the determined optimum moisture and maximum density (Figure 2). The samples were cured under humid conditions for 7 and 28 days.

Figure 1 – Preparation of soil-cement mixes

Figure 2 – Cylindrical samples from soil-cement mixes

The physical and mechanical tests of stabilized and non-stabilized samples included: determination of compressive strength under uniaxial loading according to [16] (Figure 3); evaluation of frost resistance by repeated freezing–thawing cycles at –18°C, followed by strength testing; assessment of water resistance through capillary and full water saturation tests. In addition, mineralogical studies were conducted to determine the composition of soils. Fourier-transform infrared spectroscopy was used to identify the main functional groups of minerals, while microscopic examination provided information on soil microstructure.

Figure 3 – Determination of the compressive strength of samples

The obtained results were processed statistically and compared with the requirements of the regulatory documentation [17]. The compliance of the tested compositions with these requirements was analyzed to evaluate the efficiency of the stabilizing additives.

3. Results and Discussion

Table 1 below shows the physical and mechanical properties of soils typical for the cities and regions of West Kazakhstan.

Table 1 – Physical and mechanical properties of soils

Region	Soil class	Liquid limit moisture, %	Rolling limit moisture, %	Plasticity index, %	Maximal density, g/cm^3	Optimum moisture, %
Atyrau city	Sandy loam	21.3	15.2	6.1	2.18	8.9
WKR	Sandy loam	20.6	14.85	5.75	2.25	9.09
Aktobe city	Loam	36.4	26.1	10.3	2.31	11.9
Mangystau region	Loam	32.8	18.2	14.6	2.34	11.8

The table shows that sandy loams (Atyrau city and WKR) are characterized by relatively low plasticity (plasticity index of ≤ 6.1) and optimum moisture content of ≤ 9.1%, which makes them less sensitive to moisture saturation. At the same time, loams (Aktobe city and Mangystau region) have

significantly higher liquid limit moisture values (up to 36.4%), plasticity index (from 10.3 to 14.6 %), and optimum moisture content (almost 12%). This indicates a greater variability of their structure with changes in humidity and the need for a more careful selection of stabilizers. The maximum density of loams is slightly higher (from 2.31 to 2.34 g/cm^3) compared to sandy loams (from 2.18 to 2.25 g/cm^3), which reflects their denser constitution.

The spectral analysis with the IR-Fourier spectrometer used to conduct a comprehensive assessment of the structural features of the soils revealed the presence of the main functional groups of minerals present in the samples under study. The results of the spectral analysis of the soils are presented in Table 2.

Table 2 – Mineral composition of soils in the studied areas

Region	Main minerals, %							
	O	Na	Mg	Al	Si	K	Ca	Fe
Atyrau city	48.06	0.73	1.77	4.67	34.33	1.23	4.25	4.95
WKR	44.89	1.32	8.22	26.61	26.61	2.96	10.74	5.26
Aktobe city	46.64	0.93	1.76	11.40	27.62	2.63	3.78	5.22
Mangystau region	39.64	0.67	1.93	7.74	16.74	1.68	26.19	4.82

The mineral composition of soils varies significantly across regions. In the Atyrau region, silica (Si ~34%) and oxygen (~48%) predominate, which corresponds to light sandy loams with a high quartz content. WKO soils are distinguished by an increased content of aluminum (Al ~27%) and calcium (Ca ~10.7%), which indicates admixtures of clay minerals and carbonates. Aktobe loams contain more aluminum and iron oxides (Fe ~5.2%), which determines their high plasticity. The most specific are Mangystau soils, where a significant calcium content is observed (Ca ~26%), indicating the presence of carbonate compounds that reduce plasticity and increase soil rigidity. These features are clearly visible in the microstructural images shown in Figure 4.

a) Atyrau city

b) WKR

c) Aktobe city

d) Mangystau region
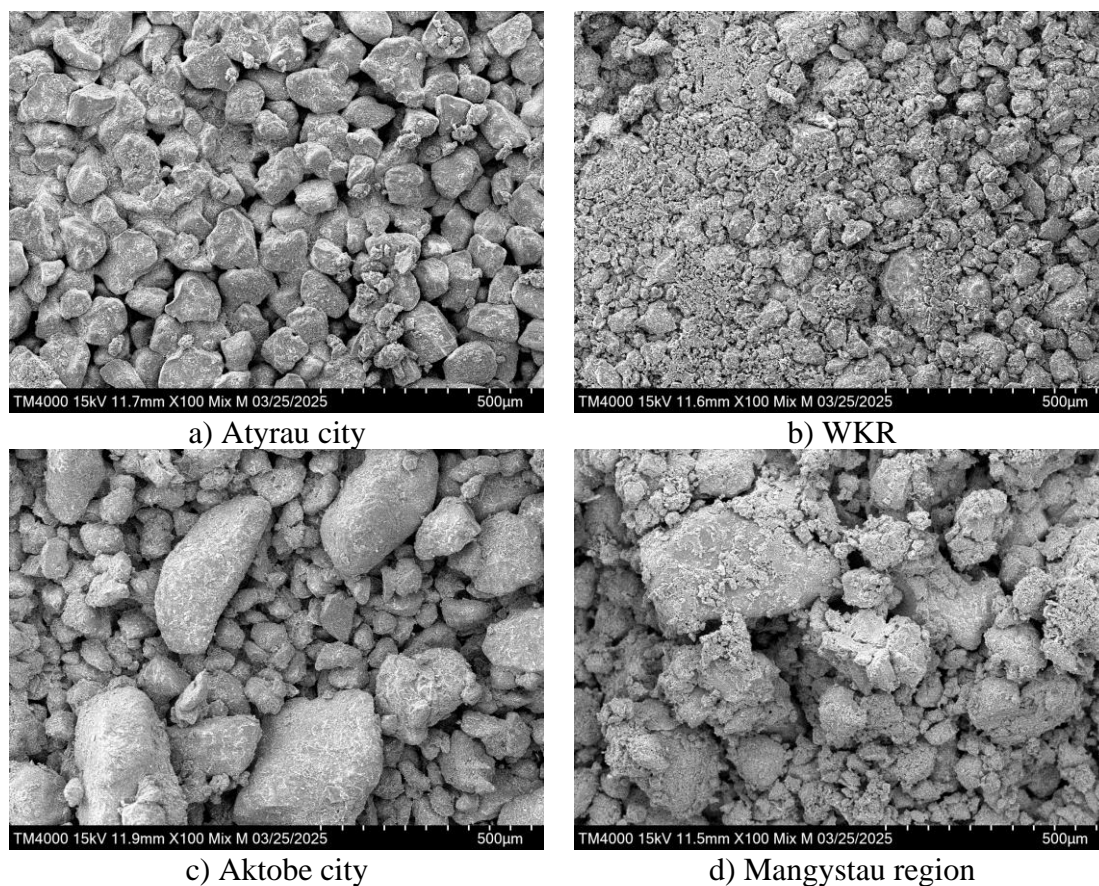
Figure 4 – Microstructure of soils under a microscope

Sand and gravel mixtures were used as inert components, providing the structure and required density of the soil base. Their use contributed to the improvement of the distribution of the modifying additive in the mixture and the stabilization of the structure of the studied samples. Both traditional and innovative additives were used to stabilize the soils: Portland cement grade M400, as well as experimental stabilizers. Individual and combined compositions were studied to increase strength, reduce water absorption, and enhance frost resistance. The results of the test for compressive strength (CS, MPa) and frost resistance (RF, cycles) of the samples are shown in Table 3.

Table 3 – Compressive strength and frost resistance of soils with various stabilizing additives

No.	Additive	Atyrau city				WKR				Aktobe city				Mangystau region			
		CS, MPa			FR,				FR,				FR,				FR,
		7 days	28 days	Grade	cycles	7 days	28 days	Grade	cycles	7 days	28 days	Grade	cycles	7 days	28 days	Grade	cycles
-	No additive	1.1	2.2	M20	F15	1.1	2.3	M20	F15	1.1	2.7	M20	F15	1.1	2.4	M20	F15
1	"EZCON" high concentration	1.4	3.6	M20	F15	2.2	4.7	M40	F25	1.6	3.7	M20	F25	1.8	4.2	M40	F25
2	"EZCON" low concentration	1.7	3.6	M20	F15	1.9	3.3	M20	F15	1.3	3.3	M20	F15	1.9	3.3	M20	F15
3	"ANT"	1.7	3.7	M20	F15	1.4	4.3	M40	F25	1.9	3.5	M20	F15	1.4	3.0	M20	F15
4	"Gistrong pul"	1.3	3.0	M20	F15	2.5	6.0	M60	F50	2.0	3.8	M20	F15	1.8	4.2	M40	F25
5	"Nova create"	1.9	4.7	M40	F25	1.8	4.3	M40	F25	1.3	2.7	M20	F15	1.9	3.8	M20	F15
6	"Gistrong"	1.9	4.1	M40	F25	1.4	3.6	M20	F15	1.5	3.1	M20	F15	2.1	4.1	M40	F25

The results of compressive strength obtained at 7 days are presented in Figure 5, while the strength values at 28 days are shown in Figure 6.
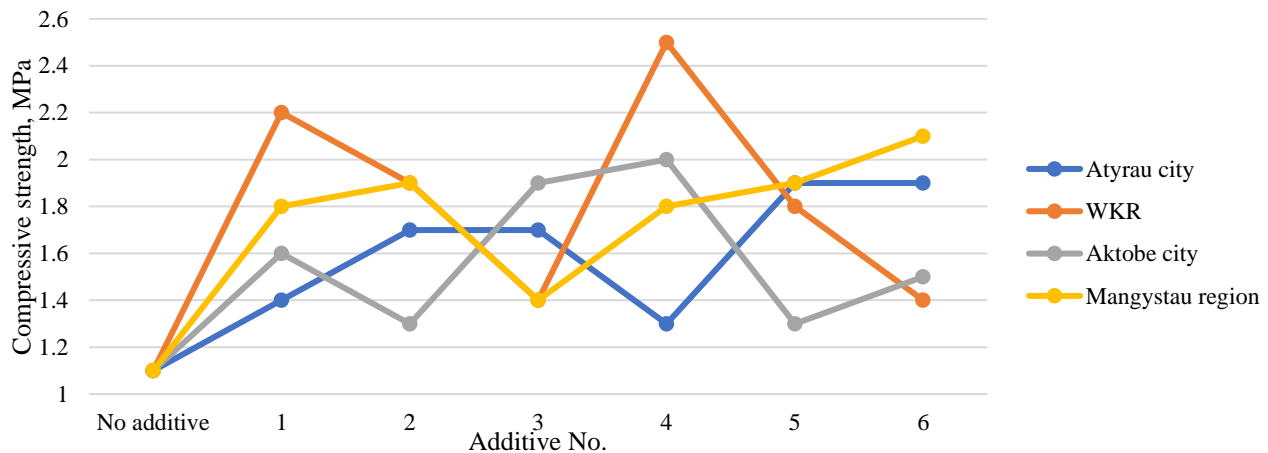
Figure 5 – Compressive strength of samples after 7 days of curing
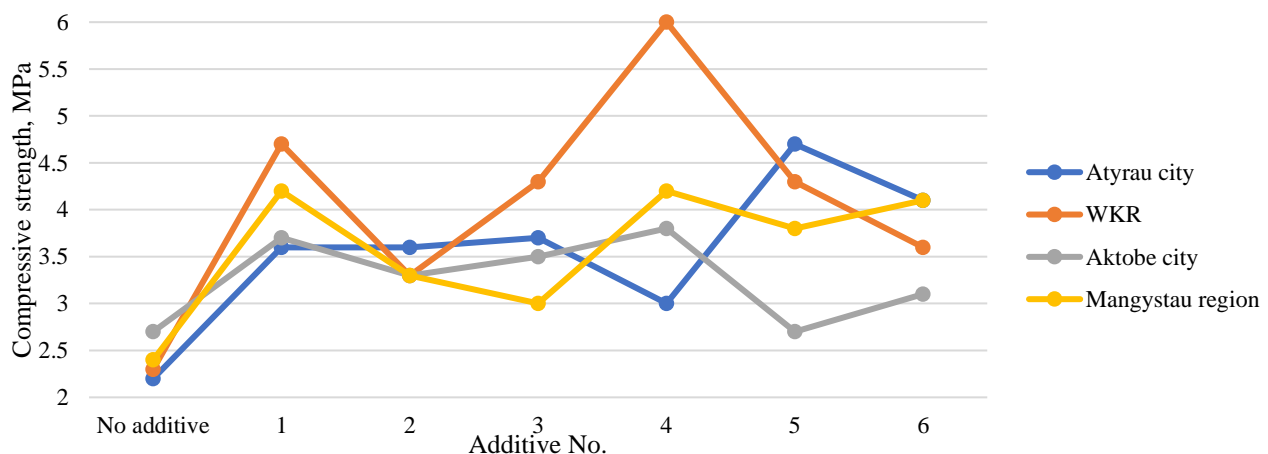
Figure 6 – Compressive strength of samples after 28 days of curing

Without additives, the strength of all soils did not exceed 2.7 MPa on the 28th day, which corresponds to a low strength grade (M20). The use of additives significantly increased the indicators. Thus, additive No. 4 in WKR turned out to be the most effective (up to 6.0 MPa, M60), indicating high compatibility with the aluminosilicate components of this soil. In the Atyrau city, additives No. 5 and 6 showed the best results (4.1-4.7 MPa, M40), which is almost twice as high as in the control. For the Aktobe city loams, the increase was less significant – a maximum of 3.8 MPa (additive No. 4), which is due to their high plasticity. The most stable results are observed in Mangystau soils: strength of 4.1-4.2 MPa (M40) with additives No. 4 and 6, which is explained by their carbonate nature. Thus, the effectiveness of stabilizers depends on the mineral composition of the soil: in carbonate and sandy loam soils, a higher increase in strength is achieved than in clay loams.

These tendencies are consistent with the results of previous studies conducted by foreign researchers. In particular, it has been shown that cement–slag systems demonstrate the highest efficiency in soils with a significant proportion of aluminosilicates [3], which corresponds to the findings obtained for WKR soils in this study. [5] noted that additives based on industrial by-products contribute to improving the durability of sandy loams, which is confirmed by the results for the Atyrau city soils. For carbonate soils, such as those in the Mangystau region, earlier research highlighted the higher effectiveness of stabilizers due to their reduced plasticity [9], which also agrees with the current results. At the same time, the relatively weak effect of additives on the Aktobe city loams is consistent with conclusions from previous studies emphasizing the strong dependence of clayey soils on mineral composition and fines content [2]. Overall, the comparative analysis confirms that soil mineralogy is the key factor determining the compatibility and efficiency of stabilizers.

4. Conclusions

The study examined the physical, mechanical, and mineral characteristics of soils in various regions of Western Kazakhstan, as well as the effectiveness of modern stabilizing additives.

1. Analysis of the physical and mechanical properties showed that sandy loams (Atyrau and West Kazakhstan regions) have relatively low plasticity and lower optimum moisture content, which makes them less sensitive to changes in the moisture regime. At the same time, loams (Aktobe and Mangystau regions) are characterized by increased plasticity and higher optimum moisture content, which requires the use of additional stabilization measures.

2. The mineral composition of the studied soils demonstrated significant differences: silica predominates in sandy loams, while WKO soils have a high content of aluminum and calcium, Aktobe soils have iron oxides, and Mangystau soils have a significant proportion of carbonates. These features determine the different reactions of soils to the use of modifying additives.

3. Compressive strength tests showed that without additives, soils in all regions have low values (up to 2.7 MPa, M20). The use of stabilizers made it possible to increase strength by 1.5–2.5 times. Additive No. 4 turned out to be the most effective in the West Kazakhstan region (6.0 MPa, M60), while additives No. 5 and 6 (up to 4.7 MPa, M40) turned out to be the most effective in the Atyrau and Mangystau regions. The increase was the smallest for Aktobe loams, which is due to their high plasticity and structural heterogeneity.

4. The comparative analysis demonstrated that the efficiency of stabilization depends primarily on soil mineralogy. Sandy loams and carbonate soils are most responsive to combined additives, showing a significant increase in strength and frost resistance. Loams with high plasticity require the development of specialized stabilizer compositions, potentially with a higher proportion of binding phases and improved dispersion technologies.

Thus, the findings highlight soil mineralogy as the determining factor for selecting stabilizers and predicting their performance. The differentiated approach to the choice of additives, depending on the mineralogical composition of soils, should become the basis for the design of durable and climate-resistant road foundations in Western Kazakhstan.

References

[1] R. Lukpanov, S. Yenkebaev, Z. Zhantlessova, D. Dyussembinov, A. Altynbekova, and R. Rakhimov, "Assessment of the bearing capacity of variable profile piles in soil using static load model tests on a testing apparatus," *Eastern-European Journal of Enterprise Technologies*, vol. 2, no. 1 (128), pp. 6–13, Apr. 2024, doi: 10.15587/1729-4061.2024.301421.

[2] A. Musbah, M. Mohammed, and A. Alfghia, "The Effect of Mineral Composition and Quantity of Fines on the Atterberg Limits and Compaction Characteristics of Soils," *Open Journal of Civil Engineering*, vol. 14, no. 02, pp. 258–276, 2024, doi: 10.4236/ojce.2024.142014.

[3] L. Liu, A. Zhou, Y. Deng, Y. Cui, Z. Yu, and C. Yu, "Strength performance of cement/slag-based stabilized soft clays," *Constr Build Mater*, vol. 211, pp. 909–918, Jun. 2019, doi: 10.1016/j.conbuildmat.2019.03.256.

[4] A. Zhussupbekov, A. K. Zhankina, A. S. Tulebekova, A. Yessentayev, and I. Zhumadilov, "Features of the bearing capacity estimation of the collapsing soil bases," *International Journal of GEOMATE*, vol. 22, no. 92, Apr. 2022, doi: 10.21660/2022.92.1656.

[5] B. Shinde, A. Sangale, M. Pranita, J. Sanagle, and C. Roham, "Utilization of waste materials for soil stabilization: A comprehensive review," *Progress in Engineering Science*, vol. 1, no. 2–3, p. 100009, Oct. 2024, doi: 10.1016/j.pes.2024.100009.

[6] R. Lukpanov, D. Dyussembinov, S. Yenkebaev, D. Tsygulyov, and M. Karacasu, "Complex additive for improving the strength properties of heavy concrete based on industrial waste," *Technobius*, vol. 4, no. 4, p. 0067, Oct. 2024, doi: 10.54355/tbus/4.4.2024.0067.

[7] M. Y. Yerzatova, K. K. Mukhambetkaliev, A. Jumabayev, and A. Tlegenov, "Enhancing the Load-Bearing Capacity and Stability of Weak Soils: An Evaluation of Soil Improvement Techniques," 2025, pp. 1–8. doi: 10.1007/978-3-031-82938-3_1.

[8] A. Tulebekova, Z. Kusbergenova, B. Dosmukhambetova, T. Abilmazhenov, and I. Zhumadilov, "Study of the impact of biopolymer and geosynthetics reinforcement on soil strengthening," *EUREKA: Physics and Engineering*, no. 6, pp. 70–80, Nov. 2024, doi: 10.21303/2461-4262.2024.003472.

[9] A. Kayumov, B. Salimova, R. Khakimova, and A. Kayumov, "Strengthening the roadbed of highways using soil stabilizers," *E3S Web of Conferences*, vol. 264, p. 02012, Jun. 2021, doi: 10.1051/e3sconf/202126402012.

[10] S. Zh. Jumadilova, V. A. Khomyakov, A. K. Kenebayeva, and Zh. N. Moldamuratov, "The use of geosynthetic materials to increase the bearing capacity of soil cushions," *Nanotechnologies in Construction A Scientific Internet-Journal*, vol. 16, no. 4, pp. 342–354, Aug. 2024, doi: 10.15828/2075-8545-2024-16-4-342-354.

[11] A. Tulebekova, A. Zhankina, R. S. Imambayeva, B. Makhiyev, A. Khapin, and D. Anop, "A practical solution for improving soil bases in problematic engineering conditions," *International Journal of GEOMATE*, vol. 25, no. 108, Aug. 2023, doi: 10.21660/2023.108.3849.

[12] *ST RK 973-2015 Stone materials and soils treated with inorganic binders for road and airfield construction. Specifications*. Astana, Kazakhstan, 2015.

[13] *ST RK 1273-2004 Soils, methods for laboratory determination of grain (granulometric) composition*. Astana, Kazakhstan, 2004.

[14] *GOST 25100-2011 Soils. Classification*. Moscow, Russia, 2011.

[15] *ST RK 1217-2003 Sand for construction works. Test methods*. Astana, Kazakhstan, 2003.

[16] *ST RK 1290-2004 Soils. Methods of laboratory determination of physical characteristics*. Astana, Kazakhstan, 2004.

[17] *ST RK 1218-2003 Materials and products of organic binders for road and airfield construction. Test methods*. Astana, Kazakhstan, 2003.

Information about authors:

Mariya Smagulova – PhD Student, Department of Technology of Industrial and Civil Engineering, Faculty of Architecture and Construction, L.N. Gumilyov Eurasian National University, Astana, Kazakhstan, smagulovamariya98@gmail.com

Duman Dyussembinov – Candidate of Technical Sciences, Department of Technology of Industrial and Civil Engineering, Faculty of Architecture and Construction, L.N. Gumilyov Eurasian National University, Astana, Kazakhstan, dusembinov@mail.ru

Jeong Ku Kang – PhD, Adjunct Professor, Department of Civil and Environmental Engineering, Incheon National University, Incheon, Republic of Korea, jeong99k@inu.ac.kr

Adiya Zhumagulova – Candidate of Technical Sciences, Department of Technology of Industrial and Civil Engineering, Faculty of Architecture and Construction, L.N. Gumilyov Eurasian National University, Astana, Kazakhstan, zaaskarovna@gmail.com

Manarbek Zhumamuratov – Junior Researcher, Scientific Research and Development Center, JSC "Kazakhstan Road Research Institute", Astana, Kazakhstan, zhumamuratovmanarbek@gmail.com

Author Contributions:
Mariya Smagulova – concept, methodology, data collection, laboratory testing, analysis, drafting.
Duman Dyussembinov – supervision, resources, methodology, interpretation, editing.
Jeong Ku Kang – modeling, analysis, visualization, interpretation, editing.
Adiya Zhumagulova – methodology, data collection, analysis, drafting, editing.
Manarbek Zhumamuratov – resources, data collection, laboratory testing, visualization.

Conflict of Interest: The authors declare no conflict of interest.

Use of Artificial Intelligence (AI): The authors declare that AI was not used.

Article

Application of computational methods for real-time monitoring and structural integrity assessment of reinforced concrete structures

Beibit Akhmetov[*], Roza Serova, Saltanat Zhautikova

Abylkas Saginov Karaganda Technical University, Karaganda, Republic of Kazakhstan
*Correspondence: beibit.bakiuly@mail.ru

Abstract. This study develops and validates a method for real-time monitoring and structural integrity assessment of reinforced concrete facilities in Karaganda, Kazakhstan, integrating finite element modeling (FEM), machine learning (ML), and digital signal processing (DSP). Three pilot objects were analyzed: a three-span bridge, an 18-storey residential building, and a reinforced concrete highway section. FEM models built in ANSYS 2024 R1 were linked with calibrated sensor networks (strain gauges, accelerometers, thermocouples, tiltmeters, weather stations). Data processing was performed in MATLAB and SciPy, with ridge regression models ($R^2 \approx 0.85$) used for defect prediction. Results showed close correspondence between calculations and measurements: deviations of 2% for the bridge (r = 0.98) and 4% for the building (r = 0.95) met the ≤5% accuracy target. The road section produced a 25% error (r = 0.90), mainly due to frost heave and heterogeneous traffic. Cost–benefit analysis indicated net efficiency within five years, with cumulative savings of 110–120 million KZT versus 67 million KZT in costs. The findings confirm the effectiveness of integrated digital monitoring for preventive maintenance, though further validation in different climates and materials is required.
Keywords: reinforced concrete structures, defects, operation, finite element method, sensor.

1. Introduction

Structural health monitoring (SHM) uses sensor networks and computational methods to enable early damage detection and prevent accidents. The durability of reinforced concrete structures is critical for the safety and economy of regions. In this study, we combine finite element modeling (FEM), machine learning (ML), and digital signal processing (DSP) to analyze large streams of monitoring data and to predict stress–strain states under real operating conditions. The approach relies on calibrated sensor networks (strain, acceleration, temperature, tilt) and standardized material properties, with model–data synchronization ensuring that computational predictions are directly comparable to field measurements.

Traditional visual and mechanical inspections are labor-intensive and often miss hidden defects [1]. The transition to digital sensors has reduced subjectivity, but the data remains fragmented, and the models poorly reflect real operating conditions, especially with sharp temperature fluctuations and high traffic.

Mehta M. showed that manual surveys underestimate deep cracks, increasing the risk of costly reconstructions [2]. [3] improved the prediction of crack formation in RC beams by 30% relative to regression using neural networks, but did not take into account temperature drift. [4] combined FEM and topology optimization for bridge trusses, correctly predicting the redistribution of forces, although the model was not tested in situ. [5] applied FEM in the construction of a suspension bridge, identifying risk zones of cables, but synchronization with field data was performed manually. [6] trained a Gaussian process on data from 76 bridges to assess the residual life, requiring a dense observation grid. [7] developed a UAV crack detection method with a Laplace-Gauss filter (94%

accuracy) sensitive to illumination. Common unsolved problems include: accurate matching of calculated and field data, consideration of seasonal factors, and assessment of the economic efficiency of complex systems.

Despite the progress made, there is still no single platform that simultaneously integrates FEM, machine learning, and DSP in real time, provides a deviation between calculation and measurement of no more than 5% for different types of objects, and demonstrates a return on investment over a five-year horizon for regional infrastructure.

The combination of FEM models, regression methods, and frequency algorithms with a calibrated sensor network provides prediction of critical stresses and early defects of reinforced concrete structures in the Karaganda region under real operating and climatic conditions, thereby reducing total maintenance costs to an economically acceptable level.

This study aims to design and field-validate an integrated structural health monitoring workflow that combines FEM, ML, and DSP for bridges, high-rise buildings, and pavements in the Karaganda region. The workflow includes calibrated FEM models, a GPS-synchronized sensor network, standardized signal-processing and feature-extraction steps, and ridge–regression–based prediction. Its performance is evaluated by comparing model outputs with measurements on three pilot objects, reporting MAPE, standard deviation, and Pearson's r with 95% confidence intervals, and by conducting a five-year cost–benefit analysis. The paper reports the achieved accuracy for the bridge and building, analyzes the larger road error and its causes, and outlines practical improvements; broader applicability is addressed in the Limitations section.

2. Methods

The procedures are presented step by step – from the description of materials through numerical modeling and sensor network configuration to signal processing and statistical analysis - which guarantees the reproducibility of the experiment. Specific values of material properties (e.g., elastic modulus or density) are not duplicated: they are given in the relevant standards and technical data sheets.

Table 1 presents the considered study areas and materials.

Table 1 – Study areas and materials

Study area	Structural system	Concrete grade*	Steel grade*	Reference drawings
Bridge across the Sarysu River	Three-span girder bridge	B30	A500C	Karaganda City Transport Dept., 2012
18-storey residential building (rail-station district)	Reinforced-concrete frame with shear walls	B25	A400	"KazGor" Design Institute, 2008
RC-surfaced highway section Karaganda–Temirtau (km 14–18)	Continuously-reinforced pavement	B35 (overlay)	-	KazAutoZhol, 2020

*Material specifications conform to GOST 26633-2015 for concrete and GOST 5781-82 for reinforcing steel

All FEM calculations were performed in ANSYS 2024 R1 in double-precision mode; pre- and post-processing were automated by Python 3.12 scripts via the PyANSYS API. In the bridge model, the slab and supports are described by SOLID186 elements, the railings — SHELL181; the grid step is 0.25 m, and the convergence is confirmed by energy ($\leq$ 5%). The bearing pads are modeled by COMBIN14 springs with a stiffness of k = 120 MN m^{-1} [8], the loads include their own weight and the equivalent of the HL-93 automobile load according to AASHTO [5]. In the building model, the walls are specified by SHELL181, the columns and beams — BEAM188; constant vertical loads and a payload of 0.5 kPa according to SN RK 2.03-30-2019 were taken into account, the wind pressure was taken as 0.38 kPa (II wind region) [9]. The road surface was modeled using a layer-by-layer elastic scheme on PLANE182 according to [10]; the moving axial load was specified by temporary pressure spots with a step of 10 Hz, and the temperature gradient of −15…+40 °C was entered using the *LDREAD command. Stresses σ were reconstructed at the Gauss points, deformations ε were

obtained using the relationship ε = Bu [8]. Although the numerical values are presented in the Results section, the visual distribution of stresses is shown here for clarity. Figure 1 presents representative FEM contour plots for the bridge, building, and road models, highlighting the zones of maximum stress concentration and confirming the correctness of the modeling procedure.
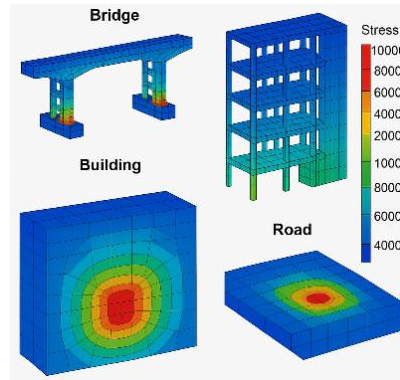
Figure 1 – FEM contour plots of stress distribution in bridge, building, and road models

Figure 1 shows typical stress concentration zones: in the bridge, they are concentrated in the nodes of supports and span slabs, in the building, in the places of connection of columns and load-bearing walls, and in the road structure, in the area of application of the wheel load. The visual coincidence of these zones with the sensor readings confirms the correctness of the constructed models and the applied methodology.

Table 2 presents the sensor network and data collection tools used.

Table 2 – Sensor network and data acquisition

Parameter	Sensor (model)	Range	Sampling freq.
Strain (bridge, building)	Vishay CEA-06-250UW-350	±5 000 με	100 Hz
Strain (pavement)	Geokon 4200	±3 000 με	10 Hz
Vibration	Brüel & Kjær 4371 ICP®	0.1–8 000 Hz	500 Hz
Tilt	GeoSIG biaxial tiltmeter	±5°	1 Hz
Temperature	OMEGA PT100 (class A)	−50 … +250 °C	1 Hz
Wheel load	Kistler 9272 piezo-quartz	0–120 kN	2 kHz
Weather	Campbell CR1000	see manual	1 min

The sensors were fixed with epoxy glue according to ASTM E251-92; measurements were recorded by NI cRIO-9045 loggers synchronized by GPS (±1 μs), and raw data were stored in TDMS format.

Signal processing was performed in MATLAB R2024b (Signal Processing Toolbox) and SciPy 1.13; filtering was performed with a fourth-order Butterworth filter with bands of 0.5–200 Hz for the bridge and building and 0.1–50 Hz for the road. Frequency analysis was performed with FFT (scipy.fft.rfft) with a resolution of 0.1 Hz. For machine learning, features of peak strains, RMS accelerations, and FFT amplitudes ≤ 100 Hz were used; the model was ridge regression ($\alpha = 1.0$) on 2000 labeled observations in scikit-learn 1.5 [11]. The input data were scaled by z-score, and hyperparameters were optimized by 5-fold cross-validation.

Statistical analysis was performed in R 4.3.2 (packages stats, psych), using the MAPE (Eq. (1)), Standard Deviation (Eq. (2)), and Pearson correlation (Eq. (3)) methods.

$$\frac{1}{n}\sum_{i=1}^{n}\left|\frac{x_i - y_i}{x_i}\right| \cdot 100\% \tag{1}$$

$$s = \sqrt{\frac{1}{n-1}\sum_{i=1}^{n}(x_i - \bar{x})^2} \tag{2}$$

$$r = \frac{\sum(x_i - \bar{x})(y_i - \bar{y})}{(n-1)s_x s_y} \tag{3}$$

95% confidence intervals for r were calculated using Fisher's z-transformation.

3. Results and Discussion

Table 3 shows the results of the comparison of the calculated FEM model with strain gauge readings.

Table 3 – Errors and agreement statistics (bridge)

Metric Value	Metric Value
Average error, %	2
Standard deviation, Pa	52.2
Correlation coefficient r	0.98

The average error is 2%, indicating almost complete agreement between the calculated and measured stresses; the small standard deviation confirms the narrow spread of the data. The correlation coefficient of 0.98 demonstrates a clear linear relationship between the FEM model results and field observations. The highest stresses are found at the beam-support nodes, and numerical modeling predicts an additional increase of 10–12% with increasing traffic and temperatures in the warm season. The obtained accuracy is consistent with the results of [5], where the discrepancy did not exceed 3%; the lower σ (52 Pa) is explained by the constant GPS synchronization of the sensors, which was absent in that study.

The summary comparison data for multi-storey residential buildings are presented in Table 4.

Table 4 – Errors and consistency statistics (buildings)

Metric Value	Metric Value
Average error, %	4
Standard deviation, Pa	141
Correlation coefficient r	0.95

The error < 5% confirms the sufficient accuracy of the models, but the increase in σ to 141 Pa is associated with variable operational loads. With the growth of useful loads and aging of the material, the calculations predict an increase in axial stresses of the load-bearing walls by 2–5%, and the tilt sensors record a gradual tilt of the two towers. The obtained correlation value (r = 0.95) coincides with the data of [3], but our average error is lower (4% versus 6%), which is explained by the integration of FEM and ML, rather than the sequential application of the methods.

The accuracy indicators of the Karaganda – Temirtau highway are given in Table 5.

Table 5 – Errors and consistency statistics (road)

Metric Value	Metric Value
Average error, %	25
Standard deviation, Pa	1187.5
Correlation coefficient r	0.90

The average error of 25% and high σ reflect diurnal variations in loads and temperatures; FFT analysis revealed a stable 50 Hz component associated with plate resonance, and the areas with the highest amplitude coincide with the cracking zone; despite the high correlation r = 0.90, the scatter exceeds the results of [6] (MAPE ≈ 15%), which is explained by the harsher climatic conditions and mixed traffic of continental Kazakhstan.

To ensure the statistical reliability of the presented indicators, 95% confidence intervals were additionally calculated using Fisher's z-transformation for correlation coefficients and bootstrapping (n = 1,000 resamples) for MAPE and σ values. For the bridge, the 95% CI for r was [0.96; 0.99], for the building [0.93; 0.97], and for the road [0.87; 0.92]. The uncertainty of MAPE values did not exceed ±0.8% for the bridge, ±1.2% for the building, and ±4.5% for the road, confirming that the observed trends remain statistically robust despite environmental variability.

Figure 2 shows a histogram of average errors: bridge - 2%, building - 4%, road - 25%; errors increase monotonically with increasing complexity of the external environment, which confirms the conclusions of [4] about the degradation of accuracy with increasing climatic and operational influences.
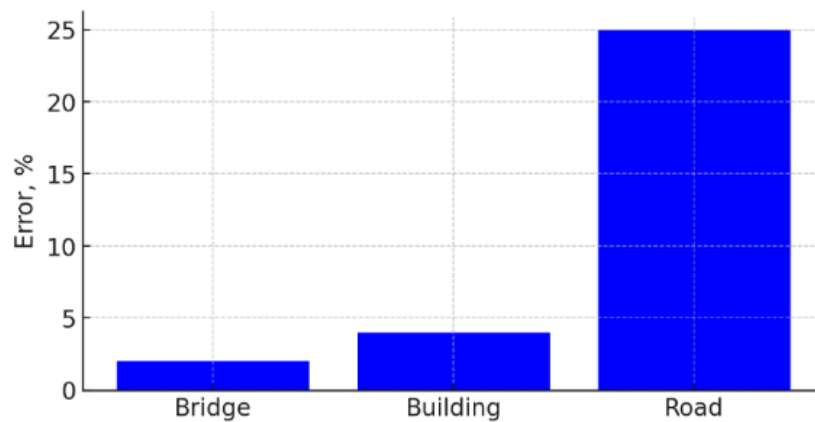
Figure 2 – Average Errors by Structure (blue bars)

The diagram in Figure 2 shows a stepwise increase in the error: from the bridge (2%) to residential buildings (4%) and then to the road (25%), which reflects the increase in the uncertainty of the calculations as the complexity of the operating environment increases; for the bridge and buildings, the accuracy is maintained ≤5% due to the relative stability of loads and microclimate, while extreme temperature changes and irregular axle loads on the road cause a quadratic increase in discrepancies; this trend confirms the findings of [4] on the degradation of the accuracy of FEM forecasts with increasing climatic and traffic impacts, and emphasizes the need for adaptive models: for bridges and buildings, the current configuration of sensors and computational schemes is sufficient, and for road surfaces, it is necessary to expand the measurement grid and complicate the numerical calculation, including temperature and traffic submodels.

The obtained error of 25% for the Karaganda–Temirtau road section indicates that, under current conditions, the model is not yet sufficiently reliable for long-term predictions. However, several strategies can reduce this discrepancy. First, increasing the density of the pavement sensor grid will allow better capturing of temperature gradients and local deformations. Second, introducing a submodel of frost heave and seasonal soil movements into the FEM scheme can address the continental climatic factors specific to Kazakhstan. Third, separating the traffic loads by axle groups (passenger cars, medium trucks, heavy trucks) and training machine learning algorithms on these disaggregated datasets will improve the predictive capability. Fourth, periodic recalibration of strain gauges and accelerometers in extreme temperature cycles will minimize measurement drift. Together, these measures will significantly reduce errors in road infrastructure models and align them with the ≤10–15% accuracy level achieved in similar studies [6].

In addition to these measures, special attention should be given to two critical factors for the continental climate of Kazakhstan: frost heave and heterogeneous traffic. Frost heave can be modeled through the introduction of a thermo-hydro-mechanical submodel within the FEM scheme, explicitly simulating soil freezing-thawing cycles, moisture migration, and their impact on pavement stiffness. For mixed traffic, disaggregated stochastic load models should be developed, where passenger cars, medium trucks, and heavy trucks are represented as separate random processes with specific axle configurations, speeds, and load spectra. Coupling these submodels with machine learning algorithms will allow the system to dynamically recalibrate forecasts, better capture seasonal nonlinearities, and reduce the observed 25% discrepancy for highways.

Figure 3 shows the open work windows of MATLAB R2024b (filtering and FFT) and VS Code running a Python script using SciPy and scikit-learn.
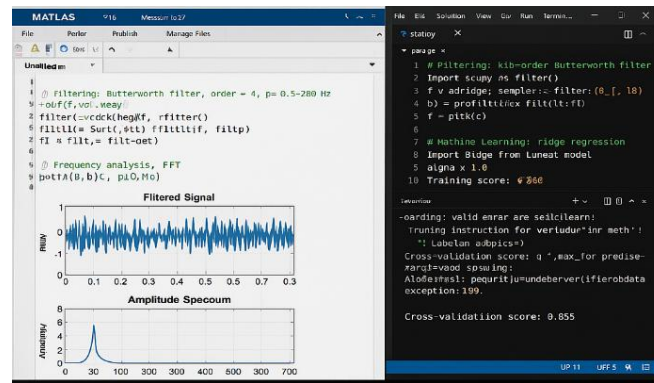
Figure 3 – Integrated analysis workspace

Dual window: MATLAB on the left shows the signal after the Butterworth filter and its FFT, and VS Code on the right shows a Python script with SciPy filtering and scikit-learn ridge regression, confirming that raw data, spectral features, and ML modeling are performed in a single workflow; instant visualization of MATLAB plots shows a "clean" signal in the passband and a dominant low-frequency peak, confirming the correctness of the filter parameters and highlighting the resonance component used further as a feature in the ML model; script automation via the Python console outputs a cross-validation score of ≈ 0.855, showing that the quality of the model is assessed in real time and corresponds to $R^2 \approx 0.85$ from the Results section; The compatibility of the tools is demonstrated by the ability to run MATLAB (commercial) and Python (open-source) on the same PC, which increases reproducibility and allows researchers to repeat DSP steps in any environment and compare the results.

Figure 3 shows a seamless signal processing + machine learning chain in which engineers filter, transform, and model monitoring data without changing context; this integration ensured low errors for the bridge and buildings and identified the need for improvements for the road surface.

The integrated discussion shows that for the bridge and buildings, the accuracy condition ≤ 5% confirms the high efficiency of the FEM + ML + DSP approach; the low σ on the bridge is related to the dense sensor network, according to [5], while the sparse network on the road requires further refinement. Ridge regression with $R^2 = 0.85$ reliably ranks the damage risk, and the frequency peak at 50 Hz confirms the laboratory resonant cracking [11], [12]. The five-year payback horizon of the digital approach is consistent with [7] calculations for UAV inspection. The largest discrepancies on the road are due to frost heave and mixed traffic; further studies should include a climate submodel and an extended ML dataset.

A more detailed economic analysis was performed to substantiate the five-year ROI claim. The cost structure includes: initial installation of sensors and loggers (≈ 42 million KZT for three pilot sites), annual calibration and maintenance (≈ 4.5 million KZT), and data processing/software licenses (≈ 3.2 million KZT per year). Expected benefits are expressed in avoided repair costs and reduced downtime: early crack detection in bridges and high-rise buildings reduces unplanned repair expenditures by ≈ 15–20%, while optimized maintenance scheduling for road pavements saves ≈ 8–12% annually. In monetary terms, this corresponds to cumulative savings of ≈ 110–120 million KZT over five years, which outweighs the total deployment cost (≈ 67 million KZT). In addition, risk mitigation (accident prevention, service continuity) provides indirect benefits that are harder to quantify but significant for policymakers.

4. Conclusions

The combined use of FEM, digital signal processing, and machine learning methods made it possible to achieve average deviations of only 2% for the bridge structure and 4% for high-rise buildings with a correlation coefficient r of at least 0.95, thereby meeting the required accuracy limit of ≤ 5%. The error on the road section was 25%, and with the increasing complexity of climatic

conditions and transport loads, it steadily increases, which indicates the need to implement adaptive models for open infrastructure systems.

The results confirmed that the integrated platform combining FEM, sensor monitoring, machine learning, and digital signal processing enables real-time detection of critical stresses and early defects in reinforced concrete structures, thereby addressing the research gap noted in the introduction.

The achieved precision opens the way to preventive maintenance: in the case of bridges and high-rise buildings, to strengthen in advance the nodes where an increase in loads is expected, and for the road surface, to rank sections according to the degree of wear and adjust the repair schedule.

The accuracy of the road model is reduced due to the excluded effects of frost heave and combined traffic flow; in addition, regular calibration of the sensors and expansion of the measurement network are necessary. To overcome the current 25% error level for highways, it is necessary to combine technical and computational improvements: 1) Expansion of the sensor grid across the pavement; 2) Integration of seasonal frost heave and moisture submodels into FEM; 3) Refinement of traffic loading schemes; 4) Systematic sensor recalibration.

In particular, frost heave can be addressed by introducing a thermo-hydro-mechanical submodel into FEM, explicitly simulating freeze–thaw cycles, moisture migration, and stiffness variations of the pavement structure. For mixed traffic, stochastic axle-load models should be incorporated, where passenger cars, medium trucks, and heavy trucks are represented as separate random processes with their own spectra of axle configurations and speeds. Coupling these submodels with machine learning will enable dynamic recalibration of forecasts and better capture seasonal nonlinearities, thereby reducing discrepancies for highways to a practically acceptable range of ≤10–15%.

The reliability of the obtained results is strengthened by confidence intervals and uncertainty estimates, which confirm that the accuracy indicators for bridges and buildings remain within the ≤ 5% target, and that the higher road discrepancy (25%) is statistically consistent with climatic and traffic variability. Furthermore, the refined cost–benefit breakdown demonstrates that the digital monitoring platform achieves net economic efficiency within a five-year horizon, with direct savings from reduced repair costs exceeding deployment and maintenance expenses. This quantitative evidence enhances the practical relevance of the approach for decision-makers in regional infrastructure management.

The generalizability of the results is limited by regional specificity: all pilot objects are located in the Karaganda region with a sharply continental climate and materials according to GOST standards. The applicability of the proposed FEM + ML + DSP platform to other climatic conditions, seismic zones, and alternative standards (Eurocode, ASTM) has not yet been verified, which requires further interregional research.

Prospects for the development of the research include:
- integration of climate and transport submodels into road surface calculations;
- expansion of training samples for machine learning algorithms;
- development of national regulations for the placement and calibration of sensors, as well as automation of data exchange between monitoring objects.

The proposed measures will improve the accuracy of forecasting and make the life cycle management of reinforced concrete facilities more efficient.

References

[1] A. Jiménez Rios, M. Georgioudakis, Y. Song, and S. Ruiz-Capel, "Editorial: Methods and applications in computational methods in structural engineering," *Front Built Environ*, vol. 9, Dec. 2023, doi: 10.3389/fbuil.2023.1339541.

[2] M. Mehta, "AFF-YOLO: A Real-time Industrial Defect Detection method based on Attention Mechanism and Feature Fusion," Oct. 19, 2023. doi: 10.21203/rs.3.rs-3449230/v1.

[3] N. Knyazeva, E. Nazojkin, and A. Orekhov, "The use of artificial intelligence to detect defects in building structures," *Construction and Architecture*, vol. 11, no. 3, pp. 18–18, Sep. 2023, doi: 10.29039/2308-0191-2023-11-3-18-18.

[4]   S. Coemert, B. Yalvac, V. Bott, Y. Sun, and T. C. Lueth, "Development and validation of an automated FEM-based design optimization tool for continuum compliant structures," *International Journal of Mechanics and Materials in Design*, vol. 17, no. 2, pp. 245–269, Jun. 2021, doi: 10.1007/s10999-020-09506-w.

[5]   T. Cho and T. S. Kim, "Probabilistic risk assessment for the construction phases of a bridge construction based on finite element analysis," *Finite Elements in Analysis and Design*, vol. 44, no. 6–7, pp. 383–400, Apr. 2008, doi: 10.1016/j.finel.2007.12.004.

[6]   Y. Okazaki, S. Okazaki, S. Asamoto, and P. Chun, "Applicability of machine learning to a crack model in concrete bridges," *Computer-Aided Civil and Infrastructure Engineering*, vol. 35, no. 8, pp. 775–792, Aug. 2020, doi: 10.1111/mice.12532.

[7]   S. Dorafshan, R. J. Thomas, and M. Maguire, "Benchmarking Image Processing Algorithms for Unmanned Aerial System-Assisted Crack Detection in Concrete Structures," *Infrastructures (Basel)*, vol. 4, no. 2, p. 19, Apr. 2019, doi: 10.3390/infrastructures4020019.

[8]   E. Prasad, "Finite Element Method: Revolutionizing Engineering Analysis," Structural Guide: Civil & Structural Engineering Knowledge Base. Accessed: Jul. 04, 2025. [Online]. Available: https://www.structuralguide.com/finite-element-method/

[9]   Z. West, "Simple Linear Regression: Modeling the Relationship Between Two Variables," Alpharithms. Accessed: Jul. 04, 2025. [Online]. Available: https://www.alpharithms.com/simple-linear-regression-modeling-502111/

[10] T. M. Atanackovic and A. Guran, "Hooke's Law," in *Theory of Elasticity for Scientists and Engineers*, Boston, MA: Birkhäuser Boston, 2000, pp. 85–111. doi: 10.1007/978-1-4612-1330-7_3.

[11] B. Rust and D. Donnelly, "The fast Fourier transform for experimentalists. Part III. Classical spectral analysis," *Comput Sci Eng*, vol. 7, no. 5, pp. 74–78, Sep. 2005, doi: 10.1109/MCSE.2005.103.

[12] T. M. Peters and J. H. T. Bates, "The Discrete Fourier Transform and the Fast Fourier Transform," in *The Fourier Transform in Biomedical Engineering*, Boston, MA: Birkhäuser Boston, 1998, pp. 175–194. doi: 10.1007/978-1-4612-0637-8_6.

Information about authors:
Beibit Akhmetov – PhD Student, Senior Lecturer, Abylkas Saginov Karaganda Technical University, Karaganda, Republic of Kazakhstan, beibit.bakiuly@mail.ru
Roza Serova – Candidate of Technical Sciences, Associate Professor, Abylkas Saginov Karaganda Technical University, Karaganda, Republic of Kazakhstan, roza_serova@mail.ru
Saltanat Zhautikova – MSc, Senior Lecturer, Abylkas Saginov Karaganda Technical University, Karaganda, Republic of Kazakhstan, saltynchik@mail.ru

Author Contributions:
Akhmetov Beibit Bakievich – concept, methodology, resources, testing, modeling, analysis, visualization, interpretation.
Serova Rauza Faikovna – concept, methodology, interpretation, drafting, editing.
Zhautikova Saltanat Akhatovna – data collection, drafting.

Conflict of Interest: The authors declare no conflict of interest.

Use of Artificial Intelligence (AI): AI tools were used in the process of writing this article, analyzing a large amount of information.

Article

The influence of opoka mineral additive on the physico-mechanical properties of gas-ceramics based on low-plasticity clay

Sarsenbek Montayev[1,*], Ainur Montayeva[2]

[1]Research Laboratory of Construction Materials and Technologies, Zhangir Khan West Kazakhstan Agrarian and Technical University, Uralsk, Republic of Kazakhstan
[2]Department of "Architecture and Construction", Korkyt Ata Kyzylorda University, Kyzylorda, Republic of Kazakhstan
*Correspondence: montaevs@mail.ru

Abstract. The article presents the results of scientific and experimental research on the development of highly porous gas-ceramics based on low-plasticity clay from the Rubezhinsk deposit. As a mineral additive, highly dispersed microporous siliceous rock-opoka from the Taskala deposit was used. Opoka is a lightweight, hard, microporous rock characterized by high natural porosity (55-60%) and a density of 1.3-1.5 g/cm³. Hydrogen peroxide, chemically composed of H_2O_2 (perhydrol), was employed as the foaming agent. The raw clay material contains 68% SiO_2, 11.8% Al_2O_3, 3.6% Fe_2O_3, and 5.6% CaO, and is classified as low-plasticity with a plasticity index of 6.5%. X-ray diffraction analysis revealed that the clay is predominantly composed of quartz, feldspar, calcite, and hematite, while the opoka consists primarily of amorphous silica. Experimental studies demonstrated that introducing 10-30% finely ground opoka into the clay slip reduces sedimentation of molded samples during drying from 12% (without additive) to 4% (at 30% opoka), thereby decreasing shrinkage and accelerating structural strength development by 10-15%. The resulting gas-ceramic samples exhibited average densities ranging from 565 to 785 kg/m³, compressive strength between 2.5 and 3.8 MPa, total porosity from 68.4% to 75.2%, and thermal conductivity values of 0.18–0.24 W/m·°C. These results indicate that the use of siliceous opoka significantly improves the performance characteristics of porous ceramics. Thus, the developed gas-ceramic materials combine low density, enhanced strength, and low thermal conductivity, making them suitable for use as effective structural-thermal insulation components in building envelope systems, particularly for the northern regions of Kazakhstan.
Keywords: low-plasticity clay, siliceous rock (opoka), gas-ceramics, foaming agent, bulk density, compressive strength, thermal conductivity coefficient, thermal insulation.

1. Introduction

The expansion of the product range and the increase in the production of thermal insulation and structural-thermal insulation products based on mineral raw materials is a relevant and pressing task, particularly for the northern regions of Kazakhstan. The demand of the construction sector for such materials can be partially met by developing new compositions and technologies for manufacturing individual units made of porous construction ceramics. This conclusion is supported by the availability, regional distribution, and the technical and economic accessibility of clay-based raw materials in Kazakhstan.

The creation of a highly porous structure in ceramic materials can be achieved during the preparation of the mass and the forming of the products, followed by structural fixation through firing. However, the high-temperature method of porosifying ceramic masses is more fuel- and energy-intensive and technologically complex compared to the method of porosifying clay slip. The latter approach requires scientific and technological justification, taking into account the specific mineralogical characteristics of the clay raw materials used.

This necessitates the development of construction materials science technologies aimed at increasing the production volume of cost-effective structural and thermal insulation products based on locally available mineral raw materials. Ceramic construction materials are known for a number of valuable technical properties, including durability, chemical and fire resistance, strength, environmental friendliness, and fire safety. In this regard, lightweight and cellular composites based on ceramic matrices can be considered promising materials with significant potential to improve thermal, mechanical, and other critical performance characteristics.

This approach is quite common in global practice. The study [1] examines the stabilization of silty clay in seasonally frozen regions using lime, ground granulated blast furnace slag (GGBS), and fly ash (FA) as curing agents. Laboratory tests, including UCS, freeze–thaw cycles, SEM, and XRD, identified an optimal LGF mixture ratio of 4:14:6 (lime:GGBS:FA) with 18% content, which enhanced strength through the formation of C–S–H and C–A–H compounds. A database of 270 UCS results was used to train machine learning models, where the PSO–BP model achieved the highest predictive accuracy ($R^2 = 0.982$). Analyses showed LGF and silty clay contents as the most critical factors. The research combines microstructural insights with machine learning to develop a reliable model for predicting soil strength under freeze–thaw conditions, offering practical guidance for geotechnical applications [1]. Another authors [2] investigates the use of sepiolite (SEP), a natural fibrous clay mineral, as an internal curing additive in cement pastes. Adding 2.5% SEP, particularly in the pre-absorbent state, was found to improve cement hydration, refine pore structure, and significantly enhance strength – compressive strength by 18.08% and flexural strength by 51.35%. Pre-absorbent SEP showed better dispersibility, enabling fiber reinforcement, pozzolanic activity, nucleation, and filling effects, while also providing internal curing. These improvements led to lower porosity, higher hydration degree, and increased C–S–H content, ultimately boosting both micro- and macroscopic performance. The findings highlight SEP's potential to sustainably enhance cement-based materials [2]. The paper [3] evaluates the use of sargassum ash as a mineral additive in ceramic clays to reduce raw material consumption and provide a sustainable use for stranded sargassum. Ceramic specimens with 10% and 20% ash were sintered at 800, 900, and 1000 °C and tested for physical and mechanical properties. The best results were obtained with 10% sargassum ash at 900 °C and 1000 °C, showing improved mechanical performance. A Life Cycle Assessment revealed that sintering is the main source of environmental impact, but incorporating 10% sargassum ash at 900 °C can both lower environmental impacts and enhance material performance compared to conventional ceramic clay [3]. The paper [4] explores the use of biomass ash, a byproduct of renewable energy generation, as the sole additive for stabilizing purple soil under different curing conditions. High-temperature treatment at 800 °C enabled the ash to consistently improve soil strength, with unconfined compressive strength (UCS) varying by curing environment. Under dry conditions, strength gains were linked to cementing effects from soluble salts and calcite, while under humid conditions, they were driven by mineral damage, particle contact changes, and multi-component cementation. The findings show that 800 °C-treated biomass ash can effectively reinforce purple soil, reduce water loss, and provide an environmentally sustainable method for waste ash utilization and soil stabilization [4]. The study [5] examines how Ground Granulated Blast-furnace Slag (GGBS), lime, and fly ash interact to improve the strength of gypsum soil. Soil mixtures with up to 16% additives were cured for different periods and tested. Results showed that fly ash alone did not significantly increase uniaxial compressive strength (UCS) but accelerated pozzolanic reactions. The greatest strength gain occurred at 28 days, driven by ettringite and silica gel formation, while earlier gains were due to cation exchange and flocculation. Microstructural analysis confirmed the growth of cementitious compounds (CH, CSHH, CHS, CAH, CASH) and ettringite crystals, which initially enhanced strength but later caused reductions in UCS at 56 days due to excessive crystal growth. Elemental analysis revealed shifts in Al:Si and Ca:Si ratios, with a marked Al:Si reduction at 28 days, indicating rapid cementitious compound formation. Overall, the findings highlight the complex role of curing time and additive interactions in strengthening gypsum soil [5]. [6] explores the partial replacement of Portland cement (PC) with bentonite clay (BC) to develop more sustainable concrete. Mortar samples were prepared with up to 30% BC, alongside artificial aggregates produced from

ground granulated blast furnace slag (GGBFS) and PC. After 28 days, tests showed that samples with 5% BC achieved nearly double the compressive strength (94.7% higher) and a 31.2% reduction in thermal conductivity compared to the control. However, BC levels above 15% led to a decline in both strength and thermal performance. The findings demonstrate that limited substitution of cement with natural bentonite can enhance mechanical and thermal properties while supporting sustainable construction practices [6]. [7] investigates the reuse of kaolin excavation waste—typically nine tons per ton of kaolin recovered – by solidifying it with quicklime (CaO), reactive magnesia (MgO), and sodium carbonate under early-age oven curing. Strength development was analyzed through mechanical testing, pH, porosity, FTIR, XRD, and SEM-EDX, alongside environmental impact assessments of the additives. Results showed that both CaO and MgO improved compressive strength, with MgO performing better (20.3 MPa vs. 12.2 MPa at 28 days). MgO's advantage, especially with oven curing, was linked to the formation of fibrous nesquehonite crystals and fewer micro-cracks. The findings highlight MgO as a more sustainable and effective alternative to CaO and Portland cement for clay solidification, making it a promising option for environmentally friendly construction materials.

An analysis of patent literature and previous research findings indicates the presence of positive international experience in the use of natural siliceous materials in porous ceramic technologies designed to improve the indoor microclimate in residential buildings. The challenge of improving the quality and affordability of fired cellular materials can be addressed by incorporating unconventional ceramic raw materials derived from local rock formations.

One such resource is the natural siliceous rock known as opoka from the Western Kazakhstan deposit. This study focuses on the development of effective structural-thermal insulating gas-ceramic materials produced from the most accessible low-plasticity clays and siliceous rocks – opoka.

Gas-ceramic materials are renowned for their exceptional mechanical strength and corrosion resistance, offering a wide range of applications across various industries. Moreover, the porous structure plays a crucial role in determining the properties of foamed materials. Since air has a low thermal conductivity of 0.026 W/(m·K) at 25°C – especially when compared to multicomponent glass, which ranges from 0.771 to 0.971 W/(m·K) [8], [9] – the incorporation of pores into the material matrix can significantly reduce overall thermal conductivity.

In addition, closed pores help suppress thermal radiation and convection, leading to optimized effective thermal conductivity under non-vacuum conditions. Beyond thermal benefits, closed pores also contribute to enhanced mechanical strength and reduced water absorption [10], [11], [12], [13], [14], making these materials an excellent choice for a variety of applications.

2. Methods

At the initial stage of the study, an assessment was conducted on the properties of raw materials intended for the production of ceramic products with a highly porous structure.

The object of the study was low-plasticity clay from the Rubezhinsk deposit, located in the West Kazakhstan Region (WKR).

The chemical composition of the clay raw material was determined in accordance with GOST 2642.0-81 and GOST 2642.12-81 (Table 1).

Table 1 – Chemical composition of clay from the Rubezhinsk deposit, WKR

Raw Material Name	Oxide Content, wt.% (or fully: Oxide Content, % by mass)								
	SiO_2	AL_2O_3	Fe_2O_3	CaO	MgO	Na_2O	K_2O	SO_3	etc
Clay Raw Material from the Rubezhinsk Deposit	68	11.8	3.6	5.6	1.6	1.5	2.22	-	4.8

The determination of the granulometric composition and plasticity of the clay was carried out in accordance with GOST 21216.2-93 "Clay Raw Materials. Methods of Analysis" and GOST 9169-75 "Clay Raw Materials for the Ceramic Industry. Classification" (Tables 2 and 3).

Table 2 – Granulometric composition of clay from the Rubezhinsk deposit, WKR

Raw material name	Clay particle content	Silt particle content	Sand particle content	Type of clay raw material
Clay from Rubezhinsk deposit	13.62	70.78	15.6	Dusty loam, medium-dispersed

Table 3 – Plasticity of clay from the Rubezhinsk deposit, WKR

Raw material	Plasticity limits		Plasticity index, %	Classification of clay raw material by plasticity index
	Lower liquid limit	Upper rolling limit		
Clay from Rubezhinsk deposit	22.92	16.42	6.5	Low-plasticity

The drying sensitivity coefficient of the clay was determined using a rapid method proposed by A. F. Chizhsky. This device is based on measuring the time it takes for cracks to appear on the surface of a wet clay sample when exposed to intense thermal radiation. The method is characterized by its speed and the simplicity of the apparatus design. It was found that the time required for the first cracks to appear in the studied clay was 50–60 seconds, which classifies it as highly sensitive to drying.

The determination of chemical elements was carried out using a JSM 6490LV INCA Energy-350 scanning electron microscope (OXFORD Instruments, UK) by JEOL (Japan), equipped with an HKL Basis energy-dispersive analysis system (OXFORD Instruments, UK), suitable for working with polycrystalline materials (Figure 1).

Element	Weight %	Atomic %
C	7.99	12.92
O	50.94	61.83
Na	0.64	0.54
Mg	1.41	1.13
Al	5.47	3.94
Si	19.40	13.42
K	1.66	0.82
Ca	7.58	3.67
Ti	0.28	0.11
Mn	0.08	0.03
Fe	4.54	1.58
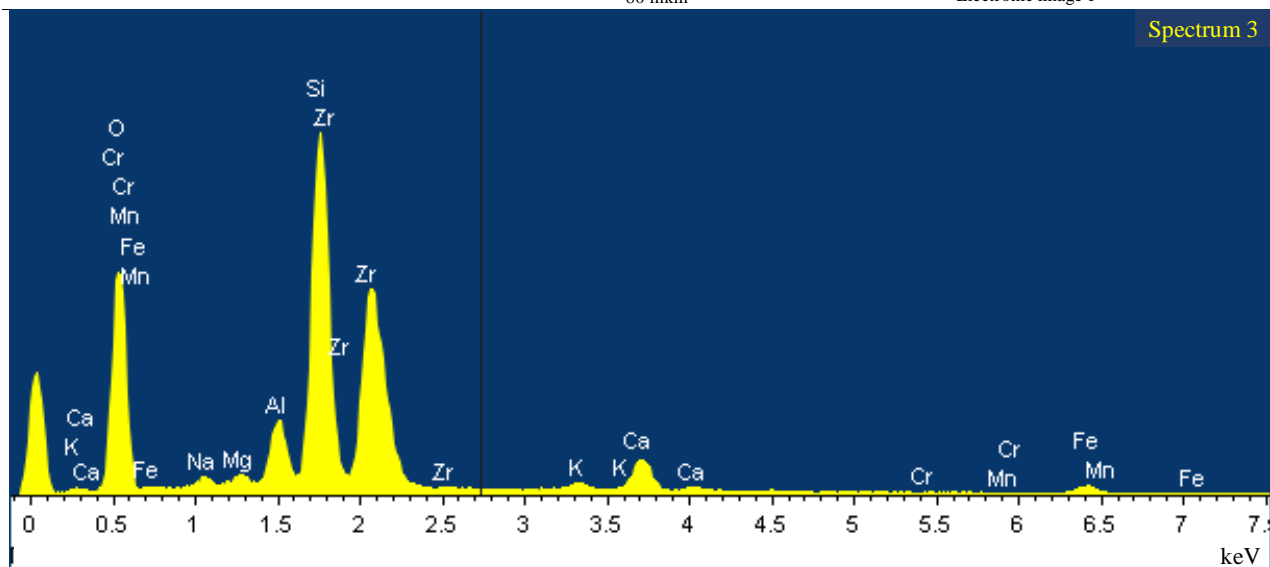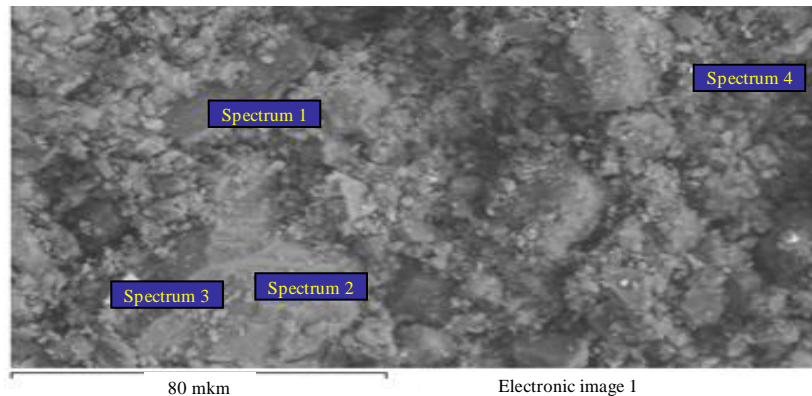
Figure 1 – Results of chemical analysis using SEM with INCA energy microanalysis system of low-plasticity clay from the Rubezhinsk deposit

The qualitative mineralogical composition of the clay was determined using the X-ray phase analysis (XRD) method on a DRON-3 diffractometer with CuKα radiation, within the angle range of 8° to 64°. The sensitivity of the method ranges from 1% to 2%. Powdered samples that passed through a 0.315 mm sieve were subjected to X-ray phase analysis. The identification of the diffraction patterns was performed using reference data [15] (Figure 2).

The interpretation of the X-ray diffraction patterns was carried out using an X-ray diffraction ruler and X-ray mineralogical identification methods based on the handbook [16].
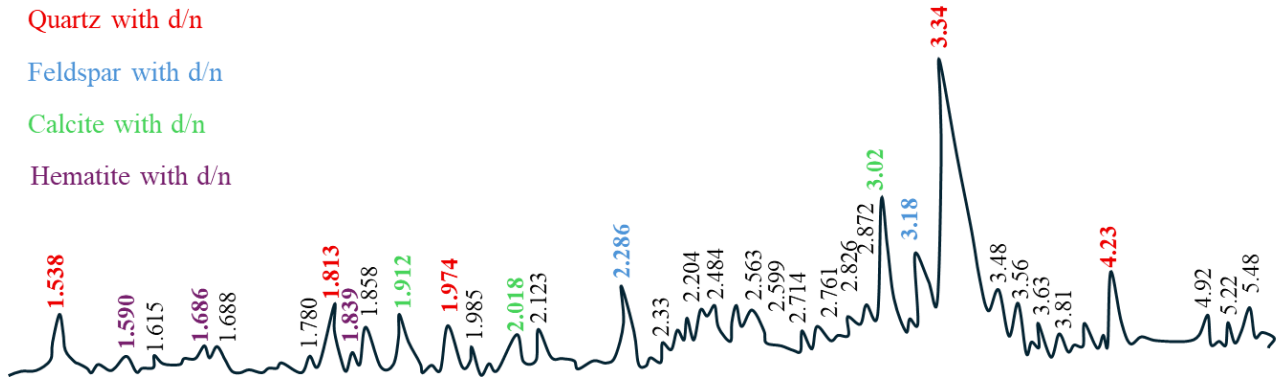
Figure 2 – X-ray diffraction pattern of low-plasticity clay from the Rubezhinsk deposit, WKR

The crystalline phases identified in the clay include quartz with d/n = 4.23, 3.34, 1.974, 1.813, and 1.538×10^{-10} m; feldspar with d/n = 3.18 and 2.286×10^{-10} m; calcite with d/n = 3.02, 2.018, and 1.912×10^{-10} m; and hematite with d/n = 1.839, 1.686, and 1.590×10^{-10} m.

Thus, it was established that the studied low-plasticity clay is predominantly composed of mixed kaolinite–hydromica mineral systems. In terms of technological characteristics, the loam is sensitive to drying and exhibits low molding properties, which may not always be favorable for the production of porous ceramics.

As a mineral additive for the production of gas-ceramics, a siliceous rock – opoka – from the Taskala deposit in the WKR was used.

The opoka from the Taskala deposit is a lightweight, hard, microporous sedimentary rock. It is characterized by high natural porosity (55-60%). According to geological data, opoka is found in Paleogene and Cretaceous formations, typically formed in marine basins through the compaction and cementation of diatomites and tripoli.

Its density ranges from 1.3 to 1.5 g/cm³. These are white or grayish, sometimes greenish lightweight rocks, occasionally containing remnants of diatom algae, radiolarians, and sponge spicules.

X-ray diffraction analysis (Figure 3) showed that the primary mineral phase is amorphous silica (SiO_2).
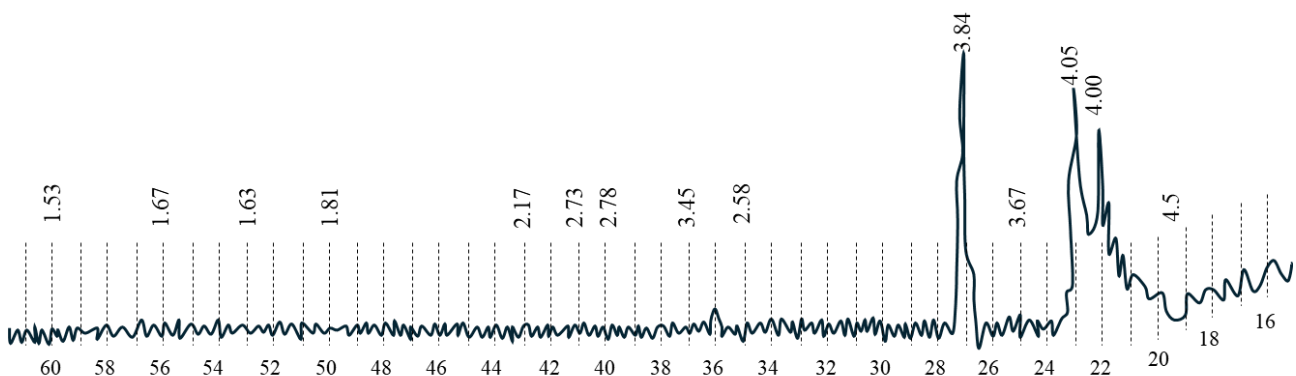
Figure 3 – X-ray diffraction pattern of the siliceous rock (opoka) from the Taskala deposit

The selection of this raw material is justified by its natural porosity and lightness, the specificity of its chemical and mineralogical composition, the presence of a large deposit in the West Kazakhstan Region, and the multifactorial influence of this additive during the stages of high-porosity ceramic production. This assertion is supported by numerous studies conducted by researchers involved in the development of porous ceramic production technologies [17], [18], [19].

Hydrogen peroxide (GOST 177-88) with the chemical composition H_2O_2 (perhydrol), medical grade, was used as the foaming agent.

To ensure the required structural integrity of the porous clay masses and the strength of the final products, it was proposed to introduce a fine mineral additive into the clay slip formulation. For this purpose, finely ground powder of the siliceous rock opoka was used.

One of the key technological operations in the production of porous ceramic materials is the preparation of the slip. In laboratory conditions, this was carried out as follows: the clay material was pre-dried and sieved through a mesh with 1 mm openings.

The additive used had a specific surface area of up to 3000 cm²/g and a microporosity of 0.8-1 cm³/g.

The mineral additive (opoka), along with 60% of the total water volume (at a temperature of 30–60°C), was mixed using a mechanical mixer for 5 minutes. Hydrogen peroxide was then added in an amount of 2-3% relative to the water content, and the mixture was stirred for an additional 1-1.5 minutes. The resulting slip was poured into molds (Figure 4), taking into account the calculated expansion coefficient. After molding, the samples were immediately dried in a laboratory drying oven at a temperature of 70-80°C until a residual moisture content of 5-7% was reached.

Figure 4 – Slip for gas-ceramic production poured into molds

The expansion coefficient was determined as the ratio of the volume of the expanded slip to the volume of the initial molding slip.

3. Results and Discussion

At the initial stage, a fine-dispersed mineral additive in the form of siliceous rock (opoka) was introduced into the slip based on low-plasticity clay in amounts ranging from 10% to 30% to study the relationship between additive content and the degree of sedimentation. For comparative analysis, a control sample consisting of slip based solely on low-plasticity clay (without additives) was used.

Figure 5 illustrates the effect of the corrective mineral additive – siliceous opoka – on the sedimentation behavior of the expanded mass based on low-plasticity clay.
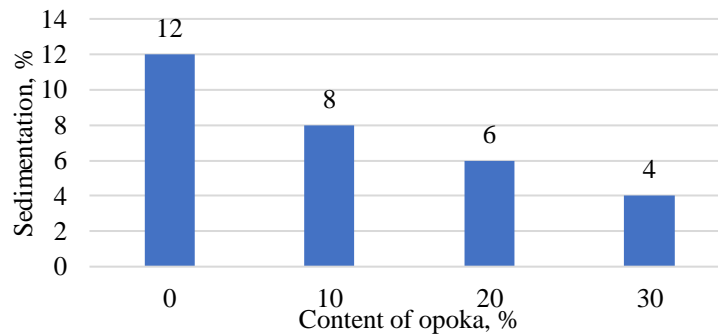
Figure 5 – Effect of the mineral additive (opoka) on the sedimentation of porous slip based on low-plasticity clay from the Rubezhinsk deposit

The research results demonstrate that the introduction of fine-dispersed, highly porous mineral additives in the form of siliceous rock (opoka) into the slip reduces the sedimentation of molded samples and the shrinkage of the products during drying. For example, the sedimentation of samples based on slip from low-plasticity clay without additives was 12%. With the addition of the mineral additive (opoka), a gradual reduction in sedimentation was observed. The maximum reduction occurred at an opoka content of 30%, resulting in a sedimentation of only 4%.

Thus, the findings at this stage of the study suggest that the incorporation of fine, highly porous siliceous mineral additives (opoka) into the slip accelerates the development of structural strength in the molding mass by 10-15% and reduces the sedimentation of molded samples during drying by 33-66%.

Figure 6 shows fragments of laboratory measurements of sample sedimentation after drying.

Figure 6 – Fragments of sedimentation measurements of porous samples after drying

After drying, the porous samples were fired in a laboratory muffle electric furnace at a temperature of 1000 °C, with a heating rate of 100 °C per hour and a holding time of 1 hour at the peak temperature. Upon completion of the firing process, the samples were cooled inside the switched-off furnace to room temperature.

Figure 7 presents the general appearance of the samples before and after firing.

a) After drying, before firing   b) After firing at t = 950 °C
Figure 7 – Gas-ceramic samples

The fired samples were tested to determine their physico-mechanical properties. The results of the physico-mechanical tests are presented in Table 4.

Table 4 – Physico-mechanical properties of gas-ceramic samples

Composition No.	Average density, kg/m³	Compressive strength, MPa	Total porosity, %	Thermal conductivity, W/m·°C
1	785	2.5	68.4	0.24
2	715	2.7	71.2	0.22
3	680	3.1	73.4	0.20
4	565	3.8	75.2	0.18

The technology for producing gas-ceramic porous materials is continuously being improved in many countries through the incorporation of various mineral additives [20], [21], [22], [23].

However, in Kazakhstan, research on the development of highly porous gas-ceramic materials using siliceous rock (opoka) from the WKR remains limited and insufficiently explored.

As the results of this study show, the addition of a highly porous, fine-dispersed mineral additive in the form of siliceous opoka to low-plasticity clay slip has a positive effect on the physico-mechanical properties of gas-ceramics.

In particular, the inclusion of 10% to 30% of this mineral additive reduces the average density of the material from 785 kg/m³ to 565 kg/m³, representing a 28.8% decrease compared to samples made from clay slip without the additive.

The mineral additive also contributes to an increase in the total porosity of the samples, from 68.4% to 75.2%, which constitutes an increase of 9.0% to 10% relative to the control samples.

In addition, improvements were observed in compressive strength and reductions in thermal conductivity. Specifically, the compressive strength increased from 2.5 MPa to 3.8 MPa, while the thermal conductivity decreased from 0.24 W/m·°C to 0.18 W/m·°C compared to the clay slip samples without the additive.

This effect is likely attributed to the high natural porosity of the siliceous opoka and its ability to undergo sintering under firing temperatures [24], [25], [26].

The findings of this study are in good agreement with the work of researchers focused on the development of highly porous ceramics from various raw material sources [27], [28], [29].

Across the literature review, two distinct pathways to sustainable construction materials emerge: (i) lightweight porous ceramics for thermal efficiency and (ii) chemically solidified or modified binders/soils for mechanical capacity. In this study, low-plasticity Rubezhinsk clay, enhanced with 10–30% Taskala opoka (amorphous-silica-rich, highly porous), produced fired gas-ceramics with very low density (565–785 kg/m³), high total porosity (68–75%), and low thermal conductivity (0.18–0.24 W/m·°C) at modest compressive strengths (2.5–3.8 MPa). Opoka cut drying sedimentation by 33–66% and accelerated structure build-up, with 20–30% opoka giving the best strength–insulation balance – an envelope-grade material ideally suited to cold climates.

By contrast, the binder/soil route prioritizes strength and durability. The LGF (lime–GGBS–fly ash) system for freeze–thaw–affected silty clays identified an optimal 4:14:6 mix at 18% content; microanalysis showed synergistic C–S–H/C–A–H formation, and a PSO–BP model ($R^2 \approx 0.982$) accurately predicted UCS under cyclic freezing, highlighting LGF and clay contents as dominant factors. For gypsum soils, lime+GGBS with fly ash improved UCS most at 28 days via ettringite and silica gel growth, while overgrowth at 56 days reduced strength—underscoring time-dependent sulfate chemistry. Biomass-ash stabilization of purple soil, after 800 °C treatment, strengthened soil across curing regimes via salt/calcite cementation (dry) and multi-component bonding with mineral damage/re-contact (humid), demonstrating a cement-free valorization path. Kaolin excavation waste solidified with MgO or CaO (early oven curing) achieved far higher 28-day strengths (≈20.3 vs 12.2 MPa) than the porous ceramics here; MgO's advantage came from fibrous nesquehonite and fewer micro-cracks, marking it a greener alternative to CaO/PC for waste-to-binder conversion.

Within cementitious composites, sepiolite at 2.5% (pre-absorbent) acted as an internal-curing, fiber-reinforcing, and nucleation agent, raising compressive and flexural strengths by ~18% and ~51% and refining pores. Bentonite as a partial PC replacement delivered an optimum at ~5% (≈95% strength gain vs control and ~31% lower thermal conductivity when combined with cold-bonded GGBFS aggregates), but >15% bentonite degraded properties—illustrating dosage sensitivity. Sargassum ash in ceramics favored 10% at 900–1000 °C, improving mechanics while LCA flagged sintering energy as the dominant impact.

Taken together, this study's opoka-modified gas-ceramics provide superior insulation at low density for building envelopes, while the other works deliver higher structural strengths, freeze–thaw resilience, internal curing, and waste valorization through chemically driven densification. The portfolios are complementary: use this study's materials where thermal efficiency and light weight are paramount, and deploy the binder/soil and composite strategies where load-bearing capacity, durability under environmental cycles, or maximum waste utilization are the primary objectives.

4. Conclusion

Based on the results of the conducted research, the following conclusions can be drawn regarding the potential of low-plasticity clay and siliceous rock (opoka) as raw materials for the production of porous gas-ceramic materials:

1) The low-plasticity clay from the Rubezhinsk deposit contains 68% SiO_2, 11.8% Al_2O_3, 3.6% Fe_2O_3, and 5.6% CaO, with a plasticity index of 6.5%, classifying it as low-plasticity. It is sensitive to drying (cracking begins after 50–60 s). XRD analysis revealed quartz, feldspar, calcite, and hematite as the main crystalline phases. The siliceous rock (opoka) from the Taskala deposit is characterized by a density of 1.3-1.5 g/cm^3 and high natural porosity of 55–60%, with amorphous silica as the dominant phase.

2) The addition of finely dispersed opoka (10–30%) to the clay slip reduced sedimentation of molded samples during drying from 12% (without additive) to 4% (with 30% opoka), i.e., a reduction by 33–66%. It also accelerated the development of structural strength in the molding mass by 10-15%.

3) The fired gas-ceramic samples exhibited average densities of 565–785 kg/m^3, compressive strength of 2.5-3.8 MPa, total porosity of 68.4-75.2%, and thermal conductivity of 0.18-0.24 W/m·°C.

4) Samples with 20-30% opoka demonstrated the most favorable balance of low density (565–680 kg/m^3), increased strength (up to 3.8 MPa), and minimum thermal conductivity (0.18 W/m·°C), confirming the effectiveness of siliceous additives in enhancing the structural and insulating performance of porous ceramics.

5) The combination of high porosity, low thermal conductivity, and adequate mechanical strength makes the developed gas-ceramic materials suitable for use as structural-thermal insulation components in building envelope systems, particularly in cold climates such as the northern regions of Kazakhstan.

References

[1] Y.-D. Sun *et al.*, "A machine learning-assisted method for evaluating the strength of silty clay solidified with industrial waste under freeze-thaw cycles," *Construction and Building Materials*, vol. 493, p. 143070, Sept. 2025, doi: 10.1016/j.conbuildmat.2025.143070.

[2] H. Zeng, X. Zhang, X. Lan, Y. Yin, and X. Chang, "Effect of sepiolite as a new greener additive on the microstructure and nanomechanical properties of cement-based materials," *Construction and Building Materials*, vol. 491, p. 142780, Sept. 2025, doi: 10.1016/j.conbuildmat.2025.142780.

[3] I. M. Da Silva Parente, G. P. Lyra, C. Bueno, F. G. Tonin, and J. A. Rossignolo, "Holistic evaluation of ceramic clay properties with Sargassum spp. ash replacement," *Construction and Building Materials*, vol. 435, p. 136680, July 2024, doi: 10.1016/j.conbuildmat.2024.136680.

[4] Q. Zhang, Z. Lu, S. Wang, X. Yu, and W. Chen, "Utilisation of biomass ash after high-temperature treatment for strengthening purple soil under various curing conditions," *Construction and Building Materials*, vol. 435, p. 136806, July 2024, doi: 10.1016/j.conbuildmat.2024.136806.

[5] A. Parhizkar, A. Nazarpour, and N. Khayat, "Investigation of geotechnical and microstructure characteristics of gypsum soil using ground granulated blast-furnace slag (GGBS), fly ash, and lime," *Construction and Building Materials*, vol. 418, p. 135358, Mar. 2024, doi: 10.1016/j.conbuildmat.2024.135358.

[6] E. Gedik and A. Atmaca, "An experimental study investigating the effects of bentonite clay on mechanical and thermal properties of concrete," *Construction and Building Materials*, vol. 383, p. 131279, June 2023, doi: 10.1016/j.conbuildmat.2023.131279.

[7] S. Ruan, S. Liang, G. Kastiukas, W. Zhu, and X. Zhou, "Solidification of waste excavation clay using reactive magnesia, quicklime, sodium carbonate and early-age oven curing," *Construction and Building Materials*, vol. 258, p. 120333, Oct. 2020, doi: 10.1016/j.conbuildmat.2020.120333.

[8] Z. Li *et al.*, "Critical secondary resource for porous ceramics: A review on recycling of inorganic solid wastes," *Journal of the European Ceramic Society*, vol. 44, no. 15, p. 116781, Dec. 2024, doi: 10.1016/j.jeurceramsoc.2024.116781.

[9] N. Santra and N. Kayal, "Preparation of high performance porous SiC ceramic membrane support using zeolite and alumina as sintering additives," *Materials Science and Engineering: B*, vol. 303, p. 117311, May 2024, doi: 10.1016/j.mseb.2024.117311.

[10] L. Han *et al.*, "Preparation of closed pore structure of fully waste-based foam glass-ceramic for thermal insulation from waste granite, glass and marble," *Journal of Materials Research and Technology*, vol. 36, pp. 8337–8350, May 2025, doi: 10.1016/j.jmrt.2025.05.025.

[11] B. V. Talpa, V. D. Kotlyar, and U. V. Terehina, "Evaluation of siliceous opokovid rocks for the production of ceramic bricks," *Ceramic building materials*, pp. 20–22, 2010.

[12] "Features of clay opok as a raw material for wall ceramics - topic of scientific article on energy and environmental management." Accessed: July 13, 2025. [Online]. Available: https://cyberleninka.ru/article/n/osobennosti-glinistyh-opok-kak-syrya-dlya-stenovoy-keramiki-1

[13] V. D. Kotlyar, "Opoki - a promising raw material for wall ceramics," *Building materials monthly scientific-technical and production journal*, vol. 2007.-№ 2.-С. 31-33, no. M.; Stroymaterialy; 1998.

[14] X. Huang, Q. Li, Y. Wu, Y. Gao, Z. Huang, and H. Zhang, "Foam gel-casting preparation of tailings porous ceramics for thermal insulation," *Ceramics International*, Apr. 2025, doi: 10.1016/j.ceramint.2025.04.119.

[15] G. Qi *et al.*, "Development and optimization of gradient pore structured porous ceramics: Modeling, properties, and potential for industrial production in thermal insulation engineering," *Construction and Building Materials*, vol. 486, p. 142017, Aug. 2025, doi: 10.1016/j.conbuildmat.2025.142017.

[16] Y. Fei, X. Song, L. Du, Y. Wang, and Z. Du, "Study on the sintering mechanism and properties of porous ceramics prepared by silicon carbide abrasive particles with multi-mineral sintering additives and silica sols," *Ceramics International*, vol. 48, no. 19, pp. 27324–27333, Oct. 2022, doi: 10.1016/j.ceramint.2022.04.326.

[17] V. F. Zavadskyi and N. B. Putro, "Estimation and regulation of thixotropic properties of clay slurries in the production of porous ceramics." Collection of scientific papers of SibADI, 2001.

[18] Y. Gao *et al.*, "Solid waste-derived porous ceramics: Unfired foaming preparation and high-temperature thermal and sound insulation," *Chemical Engineering Journal*, vol. 516, p. 163964, July 2025, doi: 10.1016/j.cej.2025.163964.

[19] N. Montayeva, S. Montayev, A. Taudaeva, M. Ryskaliev, and S. Zharylgapov, "The use of therapeutic and heat-insulating properties of siliceous gaize in the agricultural sector of the Republic of Kazakhstan," *PEN*, vol. 9, no. 4, p. 81, Sept. 2021, doi: 10.21533/pen.v9i4.2301.

[20] S. Montayev, N. Montayeva, A. Taudaeva, M. Ryskaliyev, and S. Zharylgapov, "Investigation of the Compositional Raw Mixtures for Preparation of the Sintered Microporous Material and Mineral Feed Additives," *Evergreen*, vol. 10, no. 3, pp. 1296–1306, Sept. 2023, doi: 10.5109/7151675.

[21] "Radiometric mineral identifier, Geological portal GeoKniga." Accessed: July 13, 2025. [Online]. Available: https://www.geokniga.org/books/16471

[22] "Methodical instructions for practical exercises for the course 'Modern methods of physicochemical research' (X-ray phase analysis)." Accessed: July 13, 2025. [Online]. Available: http://articles.ukgu.kz/kk/node/16392

[23] X. Wang *et al.*, "Preparation of high-quality glass-ceramics entirely derived from fly ash of municipal solid waste incineration and coal enhanced with pressure pretreatment," *Journal of Cleaner Production*, vol. 324, p. 129021, Nov. 2021, doi: 10.1016/j.jclepro.2021.129021.

[24] J. Liu, Y. Li, Y. Li, S. Sang, and S. Li, "Effects of pore structure on thermal conductivity and strength of alumina porous ceramics using carbon black as pore-forming agent," *Ceramics International*, vol. 42, no. 7, pp. 8221–8228, May 2016, doi: 10.1016/j.ceramint.2016.02.032.

[25] W. Pabst, T. Uhlířová, E. Gregorová, and A. Wiegmann, "Young's modulus and thermal conductivity of closed-cell, open-cell and inverse ceramic foams – model-based predictions, cross-property predictions and numerical calculations," *Journal of the European Ceramic Society*, vol. 38, no. 6, pp. 2570–2578, June 2018, doi: 10.1016/j.jeurceramsoc.2018.01.019.

[26] X. Huang *et al.*, "Role of waste glass as a fluxing agent in the sintering mechanism of porous ceramic aggregates from aluminium dross," *Journal of the European Ceramic Society*, vol. 45, no. 15, p. 117587, Dec. 2025, doi: 10.1016/j.jeurceramsoc.2025.117587.

[27] R. Cui, L. Zhou, Q. Ren, L. Li, and W. Li, "Optimizing porous glass-ceramics fabricated from coal gasification fine slag: Effects of ash composition on structure and properties," *Construction and Building Materials*, vol. 489, p. 140560, Apr. 2025, doi: 10.1016/j.conbuildmat.2025.140560.

[28] L. Han *et al.*, "Preparation of closed pore structure of fully waste-based foam glass-ceramic for thermal insulation from waste granite, glass and marble," *Journal of Materials Research and Technology*, vol. 36, pp. 8337–8350, May 2025, doi: 10.1016/j.jmrt.2025.05.025.

[29] S. M. Salman and S. Gharib, "Thermal conductivity of some multicomponent silicate glasses," *Thermochimica Acta*, vol. 77, no. 1–3, pp. 227–239, June 1984, doi: 10.1016/0040-6031(84)87062-8.

Information about authors:
Sarsenbek Montayev – Doctor of Technical Sciences, Professor, Head, Research Laboratory of Construction Materials and Technologies, Zhangir Khan West Kazakhstan Agrarian and Technical University, Uralsk, Republic of Kazakhstan, montaevs@mail.ru
Ainur Montayeva – PhD, Senior Lecturer, Department of Architecture and Construction, Korkyt Ata Kyzylorda University, Kyzylorda, Republic of Kazakhstan, asmontay@gmail.com

Author Contributions:
Sarsenbek Montayev – justification of relevance, analysis of experimental data, editing, conclusion.
Ainur Montayeva – data collection, testing, methodology, visualization.

Conflict of Interest: The authors declare no conflict of interest.

Use of Artificial Intelligence (AI): The authors declare that AI was not used.

Technobius

https://technobius.kz/

Article

Eco-efficient composite cements and arbolite using burnt clay shale from the Mynaral deposit

Baurzhan Amiraliyev[1], Kuanysh Imanaliyev[1,*], Zhambul Aymenov[1],
Erzhan Kuldeyev[2], Bakhrom Tulaganov[3]

[1]M. Auezov South Kazakhstan University, Shymkent, Kazakhstan
[2]K.I. Satpayev Kazakh National Research Technical University, Almaty, Kazakhstan
[3]Tashkent University of Architecture and Civil Engineering, Tashkent, Uzbekistan
*Correspondence: kuanish.69@mail.ru

Abstract. This study investigates the potential of burnt clay shale (BCS) from the Mynaral deposit (Zhambyl region, Kazakhstan) as an active mineral additive in composite cements and arbolite. Thermal and X-ray diffraction analyses revealed progressive dehydration, decarbonation, and decomposition of kaolinite, chlorite, and calcite, with optimal activation at 900 °C. Pozzolanic activity tests confirmed maximum reactivity at this temperature. Mechanical testing showed that 10–15% BCS increased cement strength up to 51 MPa, while higher dosages reduced performance. Arbolite samples with ash-and-slag binders and controlled alkaline additives demonstrated superior density and strength, supported by SEM evidence of dense crystalline microstructures and strong binder–filler adhesion. The findings highlight BCS as an effective, eco-friendly component reducing clinker consumption and CO_2 emissions.
Keywords: arbolite, rice husks, strength, binders, composite cement, active mineral additives, clay shale.

1. Introduction

Today, the construction industry actively uses local raw materials and industrial waste to produce building materials. In this regard, the production of arbolite, a material known for over a century, is considered one of the most profitable and effective ways to recycle wood waste [1]. Arbolite is a type of lightweight concrete that uses organic components, primarily wood chips, as its filler. This makes it environmentally friendly and safe for health. The wood chips also act as a reinforcing element, providing arbolite with high bending strength. This property is superior to that of aerated concrete and cement stone. Due to this feature, additional reinforcement of walls is not required when constructing buildings made of arbolite [2].

According to [3], due to its high content of wood components, arbolite is prone to moisture absorption. To protect it from getting wet, it is necessary to either plaster or cover the exterior walls. However, it also dries quickly. Another disadvantage is the uneven surface of the blocks. Unlike aerated concrete, the porous structure of arbolite leads to a disruption in its ideal geometric shape during production. [4] considered the use of geopolymer foam concrete, a material that is expensive and difficult to produce. At the same time, [2] suggest using hemp as a thermal insulation material, which can lead to a number of problems. One of the priority areas in this area is the development and improvement of the technology for the production of arbolite, which is an effective type of lightweight concrete. It is a typical local building material. Arbolite production is based on the use of waste from logging, sawmilling, woodworking, etc. [5].

The availability of local raw materials in each region allows for the development of arbolite production for local construction needs. Wood is a scarce material in Kazakhstan, and agricultural

waste can be used as a filler for arbolite. Research and development work [3] conducted to study arbolite and improve its production technology has shown the potential for using local agricultural waste in arbolite production. Given the above, the use of rice husks as a raw material for the production of arbolite blocks appears relevant when combining them with a composite cement as a binding agent for these blocks. Such a cement should contain active mineral additives that help reduce carbon dioxide emissions during production.

Cement plants are allocated significantly larger quotas compared to gypsum and silicate plants. This is due to following reasons: firstly, cement plants are usually large, with output of up to 1.2 million tons per year; secondly, when firing the raw material mixture, consisting of 70-75% limestone, a significant amount of CO_2 is released according to the reaction $CaCO_3 \rightarrow CaO + CO_2$; thirdly, when firing cement clinker using the dry method, 100-120 kg of conventional fuel is consumed per 1 ton of clinker and, accordingly, carbon is oxidized to dioxide and CO_2 is released a lot [6]. This suggests the existence of environmental problems in cement production, and due attention should be paid to solving them; cement plants should switch to "green" technologies that do not pollute the environment with various harmful emissions. One way to make cement production more environmentally friendly is the incorporation of a mineral additive – clay shales, which are rocks of metamorphic origin [7], [8].

The active mineral additives studied in [7], [8] may allow partial replacement of the clinker component in cement grinding, which will increase production efficiency, produce environmentally friendly products, reduce flue gas emissions into the atmosphere, fill the deficit of building materials in the country, reduce its cost, and increase the export potential of the Republic. Although studied works offer important directions for decarbonization, they are limited in the detailed analysis of practical barriers, focusing on conceptual or managerial aspects, ignoring the specific engineering, economic, and technical difficulties in implementing such solutions in real production. In this regard, this study aims at improving the arbolite production technology by incorporating rice husk as a filler and burnt clay shale as an active mineral additive for a composite cement.

2. Methods

The study was carried out using three main raw materials: clay shale from the Mynaral deposit (Zhambyl region, Kazakhstan), Portland cement (PC) clinker obtained from the Sastobe cement plant (Shymkent, Kazakhstan), and natural gypsum stone from a local deposit. Representative samples were collected, quartered to obtain averaged specimens, and homogenized. The shale was preliminarily ground to pass through a No. 008 sieve to ensure uniformity. Chemical analysis of all three materials was performed by X-ray fluorescence (XRF) spectrometry [9] using a PANalytical Axiosm spectrometer (Almelo, The Netherlands), which provided the quantitative oxide composition required for subsequent evaluations.

The clay shale was further examined by differential thermal analysis (DTA) [10] on a Q-1500 derivatograph (Budapest, Hungary) in the temperature range of 20-1000 °C at a heating rate of 10 °C/min. Along with the DTA curve, thermogravimetric (TG) and differential thermogravimetric (DTG) curves were recorded to identify dehydration, dehydroxylation, and decarbonization processes characteristic of the mineral phases present.

After thermal analysis, the shale was fired in an electric furnace SNOL 7.2/1100 (SnolTherm, Narkūnai, Lithuania) at three different temperatures, 700, 800, and 900 °C, with an isothermal holding period of 20 minutes. The mineralogical transformations occurring during firing were studied using X-ray diffraction (XRD) [11] analysis on a Bruker AXS D8 (Bruker Corporation, Karlsruhe, Germany) diffractometer equipped with a Cu Kα source and Vantec PSD detector, scanning across a 2θ range of 6-70°. Phase identification was carried out with reference to the ICDD PDF database.

The pozzolanic activity of the fired shale was then determined by the classical lime absorption method [12], [13]. One gram of finely ground shale was placed into 100 mL of saturated

lime solution with a CaO concentration of 1.05-1.15 g/L. The mixture was shaken and titrated with 0.05 N HCl every two to three days over 30 days using methyl orange as an indicator. The activity was expressed as the amount of $Ca(OH)_2$ absorbed per gram of additive, which provided a quantitative measure of the reactivity of the fired material.

To evaluate the effect of shale additives on cement performance, six composite cement (CC) compositions were prepared by co-grinding clinker, gypsum (5 wt.%), and shale fired at three temperatures (700, 800, and 900 °C) in proportions ranging from 5 to 30 wt.% (Table 1). A reference cement composed of 95% clinker and 5% gypsum was also produced.

Table 1 – Composition of the studied CCs, %

Composition No.	Clinker	Gypsum	Burnt clay shale (BCS)		
			700 °C	800 °C	900 °C
Reference	95	5	-	-	-
1	90	5	5	5	5
2	85	5	10	10	10
3	80	5	15	15	15
4	75	5	20	20	20
5	70	5	25	25	25
6	65	5	30	30	30

The compressive strength of prism samples with dimensions of 40×40×160 mm was determined after 28 days of curing according to [14] and [15] standards, using a PGM-100MG4 press (Stroipribor, Chelyabinsk, Russia) at a loading rate of 2 MPa/s.

Based on the obtained composite cements, five compositions of arbolite were manufactured with rice husk as the organic filler (Table 2).

Table 3 – Composition of the studied arbolite samples, %

No.	Alumosilicate component		An aqueous solution of an alkaline component		
	Ash and slag	CC	Liquid glass	Chromepik	Alkali
1	89.25	-	8.8	1.95	-
2	90.2	-	5.9	3.9	-
3	90.77	-	5.9	-	3.33
4	92.2	-	-	7.8	-
5	96	5	-	4.0	-
6	91.5	5	-	-	3.5

Cube specimens of 100×100×100 mm in size were molded and subjected to heat-moisture treatment in a steaming chamber KUP-1 (RosPribor, Belgorod, Russia) at 70 °C, following an isothermal curing cycle of 3+3+8+3 hours to accelerate strength gain. The true density of arbolite was measured using the Le Chatelier flask [16] and compressive strength was determined after 60 hours of curing in accordance with [17].

Finally, to study the internal structure of the produced composites, microphotographs of fractured arbolite samples were obtained by scanning electron microscopy (SEM) [18]. A Zeiss LEO Supra 35 microscope operating at 20 kV. The ×1000 and ×10000 magnifications were used to examine the morphology of hydration products, the adhesion of cementitious binder to the rice husk particles, and the overall development of the microstructure that defines the performance of the arbolite.

3. Results and Discussion

Table 2 below shows the results of XRF spectrometry that revealed the chemical composition of the raw materials for the composite cement.

Table 1 – Averaged chemical composition of raw materials, wt.%

Material	Calcination losses	SiO_2	Al_2O_3	Fe_2O_3	CaO	MgO	SO_3	Other
PC clinker	0.31	18.56	3.27	3.06	55.09	1.52	5.55	5.04
Clay shale	-	70.41	10.38	3.73	5.38	0.75	0.03	9.32
Gypsum stone	20.30	2.80	0.49	traces	30.98	traces	42.80	2.63

The XRF analysis shows that Portland cement clinker is dominated by calcium oxide (55.09%), with significant contributions from silicon dioxide (18.56%) and alumina (3.27%), which are typical of clinker phases. The clay shale is characterized by a very high silica content (70.41%) combined with alumina (10.38%) and minor amounts of iron oxide (3.73%) and calcium oxide (5.38%). This composition indicates that the shale can act as a siliceous-aluminous component in cement blends. The gypsum stone exhibits a high loss on calcination (20.30%) due to its water content and is mainly composed of calcium oxide (30.98%) and sulfur trioxide (42.80%), which are characteristic of gypsum ($CaSO_4 \cdot 2H_2O$). Only trace amounts of Fe_2O_3 and MgO were detected. This confirms its role as a sulfate carrier for controlling cement setting.

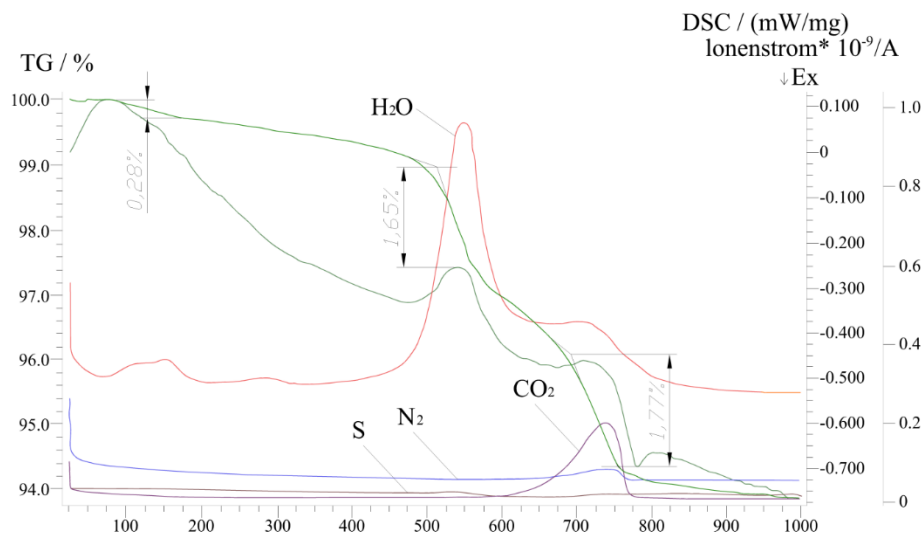Figure 1 below shows the results of the DTA of the clay shale.

Figure 1 – Thermogram of clay shale

The thermogram of clay shale demonstrates three distinct intervals of mass loss and associated thermal effects. In the temperature range of 80-170 °C, a mass loss of about 0.28% is observed, corresponding to the removal of physically bound water from clay minerals such as beidellite, halloysite, montmorillonite, and dickite. Between 530-568 °C, the second stage of dehydration occurs, resulting in a 1.65% mass loss attributed to the release of physicochemically bound water remaining in the same group of minerals. At higher temperatures, in the 700-760 °C range, a further 1.77% mass reduction is recorded, which corresponds to the loss of chemically bound crystalline water from hydroaluminosilicate minerals, including kaolinite, halloysite, and donbassite. The differential thermal and thermogravimetric curves show endothermic peaks indicating the intensity of these processes. The peak near 130 °C reflects the initial removal of absorbed moisture, which becomes most pronounced at 570 °C. A subsequent peak at 710–730 °C indicates the onset of decarbonization of calcium carbonate (calcite). Differential thermal analysis further confirms these processes, with moisture loss identified at 530–568 °C and decarbonization of calcite at around 780 °C, both accompanied by endothermic reactions. In addition, the curves show evidence of gas release, including sulfur (S), nitrogen (N_2), and carbon dioxide (CO_2), at elevated temperatures. These results are consistent with previous studies, which have shown that clay shales undergo stepwise dehydration and decarbonation processes during heating, leading to

the formation of reactive aluminosilicate phases. For instance, [19] reported that the removal of bound water from clay minerals and the decomposition of calcite above 700 °C significantly increases the pozzolanic reactivity of calcined clays.

Figure 2 below shows the results of the XRD of the fired clay shale.
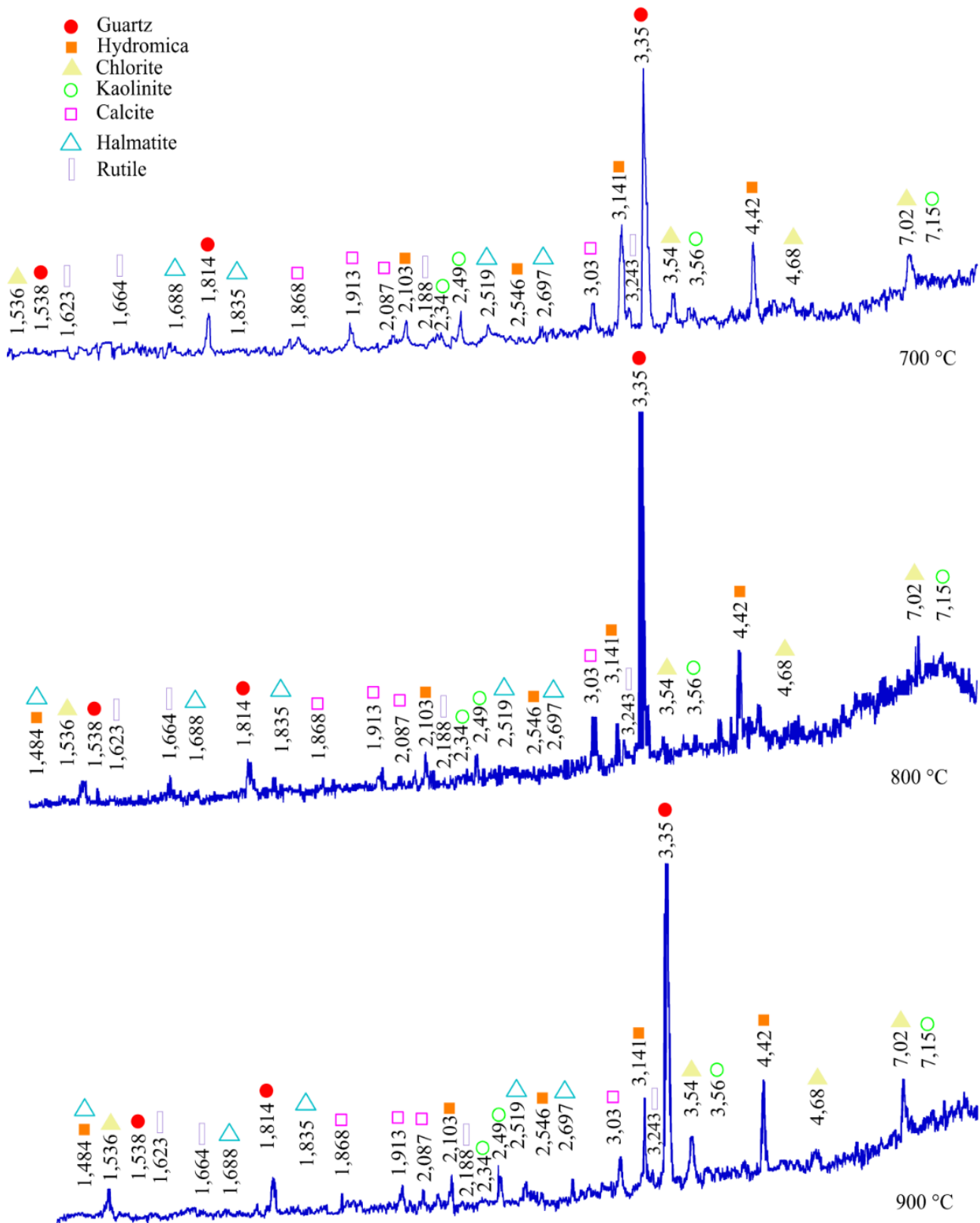

Figure 2 – XRD of fired clay shale

The X-ray diffraction patterns of clay shale fired at 700, 800, and 900 °C show significant mineralogical changes. At all three firing temperatures, the dominant reflections correspond to quartz (SiO_2) with a characteristic maximum at d = 3.35 Å. Alongside quartz, peaks of hydromica, chlorite, kaolinite, calcite, hematite, and rutile are identified. At 700 °C, reflections of kaolinite (d = 7.15, 3.56, 2.30 Å) and chlorite (d = 7.02, 4.68, 2.69 Å) remain well pronounced, indicating incomplete dehydroxylation of layered aluminosilicates. Calcite peaks (d = 3.03, 1.913, 2.087 Å) are also visible, suggesting partial retention of carbonate phases. At 800 °C, the intensity of kaolinite and chlorite reflections decreases, showing progressive breakdown of these minerals. Calcite peaks are still observed, but with reduced intensity, indicating the onset of decarbonization. Quartz reflections remain stable, while hematite and rutile are also detected. At 900 °C, kaolinite reflections almost disappear, confirming its decomposition, while quartz becomes the most stable phase. Chlorite peaks are further weakened, and calcite reflections diminish sharply, reflecting active decarbonization of carbonate minerals. The persistence of quartz and hematite at this temperature highlights their thermal stability under firing. Overall, the XRD analysis confirms that increasing firing temperature results in the gradual decomposition of clay minerals (kaolinite, chlorite, hydromica) and carbonates, with quartz remaining stable throughout, and new crystalline phases such as hematite contributing to the formation of reactive structures that enhance pozzolanic activity.

Figure 3 presents the results of pozzolanic activity tests of clay shale determined by the lime absorption method.
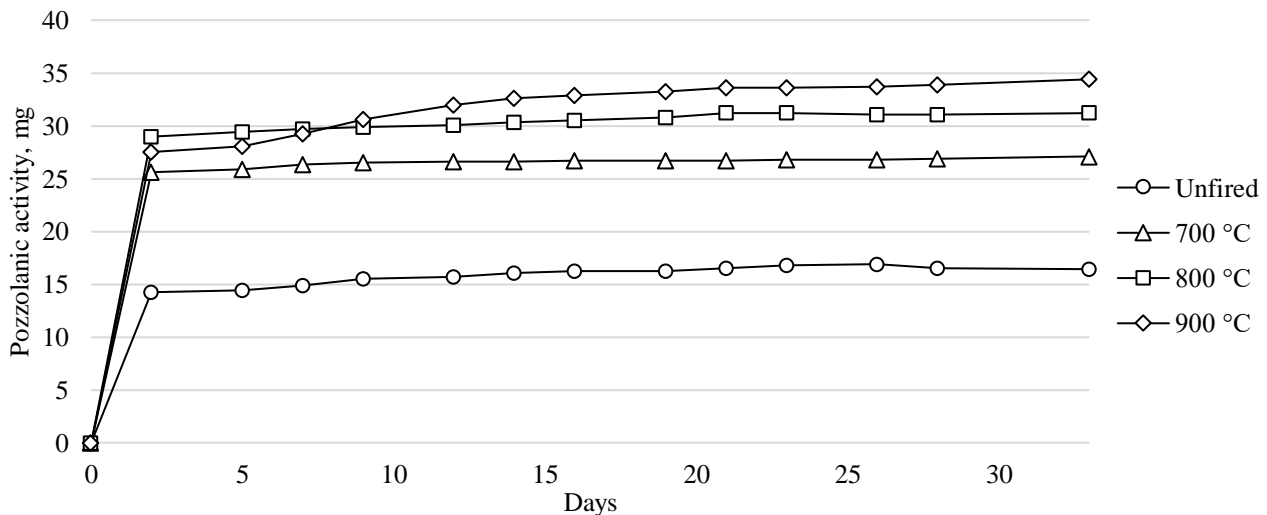
Figure 3 – Dependence of clay shale pozzolanic activity on firing temperature

The pozzolanic activity of the clay shale varies significantly depending on the firing temperature. The unfired shale shows the lowest activity, reaching only 15-18 mg of $Ca(OH)_2$ absorbed per gram of additive after 30 days. Shale fired at 700 °C exhibits moderate activity, stabilizing at about 25-27 mg. Increasing the firing temperature to 800 °C results in higher reactivity, with values rising to 30–32 mg by day 30. The maximum pozzolanic activity is observed in shale fired at 900 °C, where absorption reaches approximately 34-35 mg, demonstrating the highest lime-binding capacity. In all cases, a sharp increase in activity occurs within the first 2-3 days, followed by a gradual stabilization over the 30-day observation period. The results confirm that firing temperature plays a decisive role in enhancing the reactivity of clay shale, with optimal activity achieved at 900 °C. These findings are consistent with previous research showing that calcination significantly enhances the pozzolanic activity of clays and shales. [20] observed that thermal activation of illitic and kaolinitic clays at 900 °C leads to maximum lime consumption and improved pozzolanic performance. The observed rapid initial uptake of $Ca(OH)_2$ followed by stabilization aligns with the kinetics of pozzolanic reactions reported in these studies.

Figure 4 presents the results of compressive strength tests of composite cements with different contents of fired clay shale at 700, 800, and 900 °C.
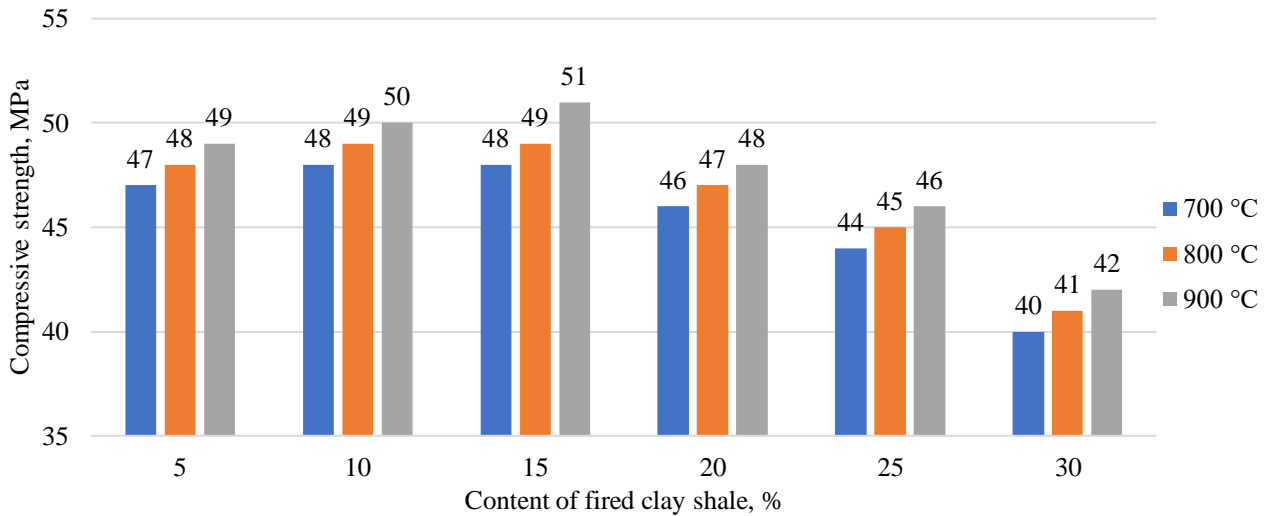
Figure 4 – Dependence of the compressive strength of the composite cement on the content and firing temperature of clay shale

The control sample without additives showed a compressive strength of 49 MPa after 28 days. When fired shale was introduced, the strength increased at additive levels of 5-15%. At 5% content, compressive strength rose slightly to 47-49 MPa depending on firing temperature. At 10% content, the values increased further to 48-50 MPa. The maximum compressive strength of 51 MPa was obtained with 15% shale fired at 900 °C, confirming this as the optimal dosage for strength gain. Beyond this level, a gradual decrease in strength was observed. At 20% content, compressive strength fell to 46-48 MPa, while at 25% it dropped further to 44-46 MPa. At the highest replacement level of 30%, strength decreased markedly to 40-42 MPa. These results indicate that while small additions of fired clay shale (up to 15%) enhance the compressive strength of composite cement, higher proportions reduce it, regardless of firing temperature. Similarly, [21] observed that optimal replacement levels of calcined clays generally lie between 10–15%, beyond which compressive strength decreases.

Figure 5 shows the results of density and compressive strength tests of arbolite samples.

Figure 5 – True density and compressive strength of arbolite

The data show that samples 1-3, which used ash and slag as the main aluminosilicate component together with liquid glass and small amounts of chromepik or alkali, achieved relatively

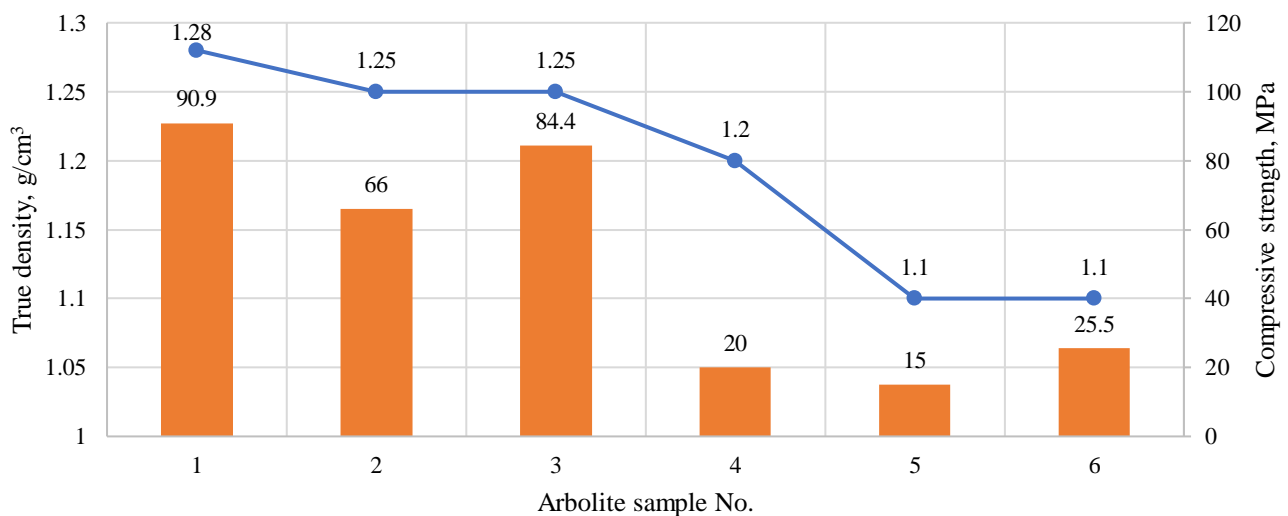high compressive strengths of 90.9, 66, and 84.4 MPa, with true densities of 1.25-1.28 g/cm³. In contrast, samples 4–6, where ash and slag were combined with larger amounts of chromepik or alkali and, in two cases, 5% composite cement, displayed much lower compressive strengths of 20, 15, and 25.5 MPa, with true density reduced to 1.1-1.2 g/cm³. These results indicate that the binder composition has a critical influence on arbolite properties: mixtures with ash and slag and liquid glass promote higher strength and density, while increasing the share of chromepik, alkali, or composite cement reduces these values markedly.

Figure 6 shows the results of SEM of the fractured arbolite based on composite cement using a clay shale.

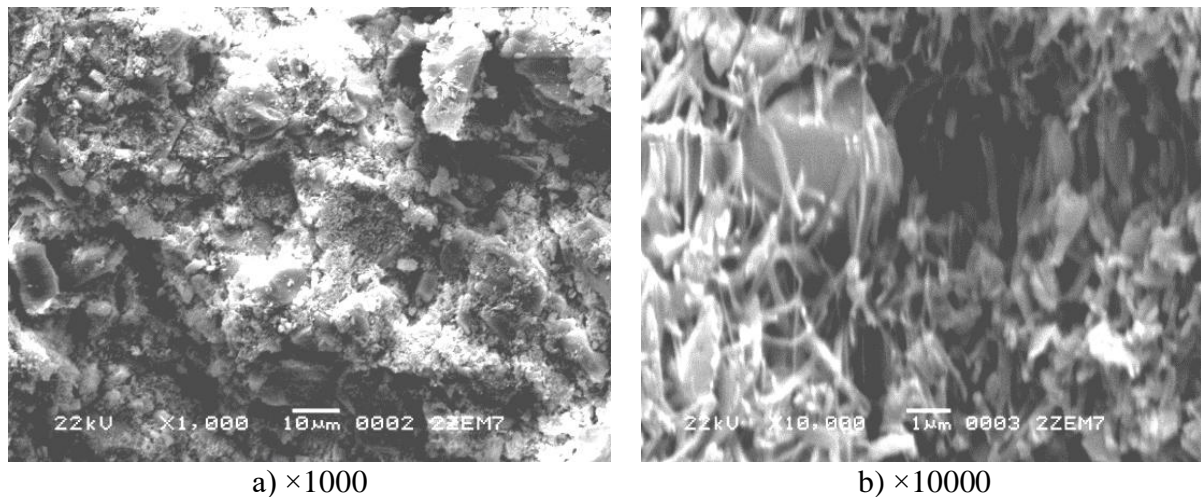a) ×1000   b) ×10000
Figure 6 – Microphotographs of fractured arbolite

The micrographs demonstrate the formation of a crystalline microstructure within the cement matrix, which serves as a framework for the material. The images confirm that hydration products are well distributed and that the structure formation process begins at the initial stages of hardening. The photographs clearly illustrate the adhesion of the binder to the organic filler, showing close contact between the cement matrix and rice husk particles. The introduction of composite cement with active mineral additives modifies the structure of arbolite, accelerating the appearance and aggregation of new formations in the microcrystalline system. The results highlight that, compared to control compositions, arbolite with composite cements develops a denser and more stable microstructure, which directly influences its strength and durability. Similar findings were presented by [22], who demonstrated that active mineral additions foster the early formation of hydration products, resulting in a more compact and durable microstructure. Future work should focus on long-term durability studies of arbolite with burnt clay shale additives under varying environmental conditions to confirm their practical performance.

4. Conclusions

The study revealed clear patterns in the behavior of clay shale and its effect on composite binders. Thermal analysis and XRD showed that structural transformations of kaolinite, chlorite, and calcite at firing temperatures up to 900 °C are directly linked to the rise in pozzolanic activity, confirming 900 °C as the optimal activation point. A consistent trend was observed in mechanical tests: moderate additions of burnt shale (10-15%) improved cement strength, whereas higher dosages reduced it due to dilution effects. In arbolite, compositions with ash-and-slag binders and controlled alkaline additives provided the best balance of density and strength, while excessive chromepik, alkali, or cement reduced performance. Microstructural analysis confirmed that these patterns result from the formation of a denser crystalline framework and improved binder-filler adhesion. Altogether, the results demonstrate that optimized use of burnt clay shale can enhance composite cements and arbolite while reducing clinker demand and environmental impact.

Acknowledgments

References

[1] M. Dlimi, R. Agounoun, I. Kadiri, R. Saadani, and M. Rahmoune, "Thermal performance assessment of double hollow brick walls filled with hemp concrete insulation material through computational fluid dynamics analysis and dynamic thermal simulations," *e-Prime - Advances in Electrical Engineering, Electronics and Energy*, vol. 3, p. 100124, Mar. 2023, doi: 10.1016/j.prime.2023.100124.

[2] B. Martínez, V. Mendizabal, M. B. Roncero, E. Bernat-Maso, and L. Gil, "Towards sustainable building solutions: Development of hemp shiv-based green insulation material," *Constr Build Mater*, vol. 414, p. 134987, Feb. 2024, doi: 10.1016/j.conbuildmat.2024.134987.

[3] K. Imanaliyev, B. Amiraliyev, K. Akmalaiuly, E. Kuldeyev, E. Yunusaliyev, and Z. Aymenov, "Research of technological parameters for producing thermal insulating arbolite based on developed slag alkali binders," *Technobius*, vol. 4, no. 3, p. 0065, Sep. 2024, doi: 10.54355/tbus/4.3.2024.0065.

[4] X. Ding, J. Yu, J. Lin, Z. Chen, and J. Li, "Experimental investigations of prefabricated lightweight self-insulating foamed concrete wall panels," *Structures*, vol. 61, p. 106001, Mar. 2024, doi: 10.1016/j.istruc.2024.106001.

[5] I. E. Kazimagomedov, L. V Trykoz, F. I. Kazimagomedov, and A. V Rachkovskiy, "Study of the forming processes of the arbolite structure during the chemical activation of flax shove," *IOP Conf Ser Mater Sci Eng*, vol. 708, no. 1, p. 012086, Dec. 2019, doi: 10.1088/1757-899X/708/1/012086.

[6] N. N. Zhanikulov *et al.*, "Receiving Portland Cement from Technogenic Raw Materials of South Kazakhstan," *Eurasian Chemico-Technological Journal*, vol. 21, no. 4, pp. 333–340, Dec. 2019, doi: 10.18321/ectj890.

[7] B. Isakulov, A. Issakulov, and A. Dąbska, "Structure Formation and Curing Stage of Arbolite–Concrete Composites Based on Iron-Sulfur Binders," *Infrastructures (Basel)*, vol. 10, no. 7, p. 179, Jul. 2025, doi: 10.3390/infrastructures10070179.

[8] B. Amiraliyev *et al.*, "Heat Treatment of Clay Shales and Their Utilization as Active Mineral Additives for the Production of Composite Cements," *Journal of Composites Science*, vol. 9, no. 6, p. 269, May 2025, doi: 10.3390/jcs9060269.

[9] *ISO 12677:2011 Chemical analysis of refractory products by X-ray fluorescence (XRF) — Fused cast-bead method*. 2011, p. 75.

[10] *ISO 11357-1:2023 Plastics — Differential scanning calorimetry (DSC)*. 2023, p. 34.

[11] D. Alderton, "X-Ray Diffraction (XRD)," in *Encyclopedia of Geology*, Elsevier, 2021, pp. 520–531. doi: 10.1016/B978-0-08-102908-4.00178-8.

[12] I. V. R. Ramanujam, K. R. Reddy, and N. V. Ramana, "Evaluation of Pozzolanic activity and lime reactivity of fly ash, GGBS, mica powder and pumice as binders," *E3S Web of Conferences*, vol. 529, p. 01008, May 2024, doi: 10.1051/e3sconf/202452901008.

[13] H. Wang, X. Liu, and Z. Zhang, "Pozzolanic activity evaluation methods of solid waste: A review," *J Clean Prod*, vol. 402, p. 136783, May 2023, doi: 10.1016/j.jclepro.2023.136783.

[14] *GOST 310.4-81 Cements. Methods of bending and compression strength determination*. 1981, p. 11.

[15] *GOST 30744-2001 Methods of testing with using polyfraction standard sand*. 2001, p. 36.

[16] *ASTM C188-17 Test Method for Density of Hydraulic Cement*. ASTM International, 2017, p. 3. doi: 10.1520/C0188-17.

[17] *GOST 10180-2012. Concrete. Methods for Determining Strength Using Control Specimens*. Moscow, Russia, 2018, p. 36.

[18] *ISO/TS 21383:2021 Microbeam analysis — Scanning electron microscopy — Qualification of the scanning electron microscope for quantitative measurements*. 2021, p. 59.

[19] E. Güneyisi, M. Gesoğlu, Özturan T., and K. Mermerdaş, "Comparing Pozzolanic Activity of Metakaolin and Calcined Kaolin, and Their Effects on Strength of Concrete," in *10th International Congress on Advances in Civil Engineering (ACE 2012)*, Ankara, Turkey : Middle East Technical University, 2012, pp. 1–10.

[20] A. Tironi, M. A. Trezza, A. N. Scian, and E. F. Irassar, "Assessment of pozzolanic activity of different calcined clays," *Cem Concr Compos*, vol. 37, no. 1, 2013, doi: 10.1016/j.cemconcomp.2013.01.002.

[21] J. Ambroise, M. Murat, and J. Péra, "Hydration reaction and hardening of calcined clays and related minerals V. Extension of the research and general conclusions," *Cem Concr Res*, vol. 15, no. 2, 1985, doi: 10.1016/0008-8846(85)90037-7.

[22] R. Walker and S. Pavía, "Physical properties and reactivity of pozzolans, and their influence on the properties of lime-pozzolan pastes," *Materials and Structures/Materiaux et Constructions*, vol. 44, no. 6, 2011, doi: 10.1617/s11527-010-9689-2.

Information about authors:
Baurzhan Amiraliyev – PhD Student, Department of Silicate Technology and Metallurgy, M. Auezov South Kazakhstan University, Shymkent, Kazakhstan, badam777@inbox.ru
Kuanysh Imanaliyev – Candidate of Technical Sciences, Associate Professor, Head of the Department of Architecture and Urban Planning, M. Auezov South Kazakhstan University, Shymkent, Kazakhstan, kuanish.69@mail.ru
Zhambul Aymenov – Doctor of Technical Sciences, Professor, Director of the Research Institute of Natural and Technical Sciences, M. Auezov South Kazakhstan University, Shymkent, Kazakhstan, zhambul_ukgu@mail.ru
Erzhan Kuldeyev – Candidate of Geological and Mineralogical Sciences, Professor, Vice-Rector for Science and Corporate Development, K.I. Satpayev Kazakh National Research Technical University, Almaty, Kazakhstan, e.kuldeyev@satbayev.university
Bakhrom Tulaganov – PhD, Rector, Tashkent University of Architecture and Civil Engineering, Tashkent, Uzbekistan, bahrombek@gmail.com

Author Contributions:
Baurzhan Amiraliyev – data collection, testing, concept, methodology.
Kuanysh Imanaliyev – concept, resources, supervision, analysis.
Zhambul Aymenov – funding acquisition, drafting, editing.
Erzhan Kuldeyev – resources, drafting, editing.
Bakhrom Tulaganov – analysis, visualization, data processing.

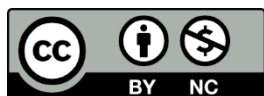**Conflict of Interest:** The authors declare no conflict of interest.

Use of Artificial Intelligence (AI): The authors declare that AI was not used.

Article

Refined methodology for the analysis of beams on elastic foundations

Sungat Akhazhanov[1], Nikolai Vatin[2], Abai Kasimov[3], Aigerim Kassenova[3,*]

[1]Research Laboratory Applied Mechanics and Robotics, Karaganda Buketov University, Karaganda, Kazakhstan
[2]Scientific and Technological Complex "Digital engineering in civil construction", Peter the Great St. Petersburg Polytechnic University, St. Petersburg, Russia
[3]Department of Building Materials and Technologies, Abylkas Saginov Karaganda Technical University, Karaganda, Kazakhstan
*Correspondence: kasenova.aigerim@mail.ru

Abstract. The study proposes a refined method for analyzing beams on a two-parameter elastic foundation, overcoming the limitations of the classical Winkler model. Unlike the traditional approach, which considers soil deformation only in the applied load zone, the proposed methods introduce an additional parameter of bending stiffness, providing a more accurate description of beam-foundation interaction. A governing differential equation was derived, and its analytical solutions are presented for various boundary conditions and loading types. The numerical analysis results show that the distribution of vertical displacement, bending moment, and shear force along the normalized length of the beam is symmetric with respect to the midspan. It has been established that the maximum values of vertical displacement and bending moment are observed at the midspan: the vertical displacement reaches 0.000999157, while the bending moment attains 0.124892. At the same time, the shear force reaches its maximum value near the beam supports, amounting to 0.49966. The results indicate that the stress-strain state critical points of the beam on an elastic foundation are concentrated at the midspan (for displacement and bending moment) and at the supports (for shear force). The analysis demonstrates that the maximum shear stresses occur near the fixed end of the beam ($x = 0$, $z = 0$), gradually decrease to zero at midspan, and reach negative values at the opposite end ($x = 1$, $z = 0$). The normal stresses vary linearly along the cross-sectional height, from negative in the lower zone ($x=1/2$, $z = -1/2$) to positive in the upper zone ($x=1/2$, $z = 1/2$), with values close to zero near the neutral axis ($x=1//2$, $z = 0$). Comparison with the classical Winkler model shows close agreement in displacements, bending moments, and shear forces, while the proposed method provides improved accuracy in predicting normal and shear stress distributions.
Keywords: beam, two-parameter elastic foundation, Winkler model, displacement, bending moment, shear force, normal stress, shear stress.

1. Introduction

The analysis of the stress-strain state (SSS) of structural elements interacting with elastic foundations remains a fundamental and practically significant problem in structural mechanics. Beams on elastic foundations are widely used in civil engineering, transportation infrastructure, mechanical engineering, and related fields, where the effect of the supporting medium on structural performance must be incorporated into design models. Accurate evaluation of internal stresses, particularly normal and shear components, is crucial for ensuring strength and serviceability of structural elements, thereby improving the reliability of engineered systems. However, classical models tend to oversimplify the representation of the elastic foundation, which significantly reduces the accuracy and reliability of practical analysis [1].

The object of this study is a beam resting on a two-parameter elastic foundation and subjected to distributed loading, a structural system widely used in civil and transportation infrastructure. This issue becomes especially important under distributed loading, typical of real operating conditions,

where complex stress distributions may arise in beams with variable stiffness, multilayer configurations, or those supported by elastic foundations.

Classical analytical approaches, such as Winkler's foundation model, assume a homogeneous medium and disregard shear stresses, which limits their applicability for realistic SSS assessment. However, distributed loading may generate complex stress distributions, especially in beams with variable stiffness, multilayer configurations, or those supported by heterogeneous foundations. Contemporary design practice, therefore, requires advanced models that account for both normal and shear stresses, interlayer interactions, and variable foundation properties. In this context, many recent contributions by different researchers have introduced refined formulations and numerical approaches to enhance the accuracy of SSS analysis and extend the applicability of theoretical models to practical engineering structures. The use of semi-analytical and numerical analytical methods, including the Ritz-Timoshenko approach and the contact layer method, enhances the accuracy of stress analysis and allows for adaptation to real engineering conditions [2]. Therefore, the topic of the present study is both timely and of considerable practical significance.

The theoretical background of this problem was established in the classical works of Winkler, Inglis, Bolotin, Timoshenko, and Muravskii, where linear models of elastic foundations and simplified loading schemes were introduced. Winkler's classical model, which assumes a linear relationship between load and settlement, has been extensively applied in engineering practice; however, the foundation is generally considered homogeneous [3], [4]. Fundamental contributions to the theory of beams on elastic foundations have addressed distributed loading, stability, and vibration problems, while also refining beam models to account for shear deformation. These developments significantly expanded the applicability of classical approaches to more realistic engineering conditions [5].

Subsequent studies by Levontev, Vlasov, and other researchers [6], [7] proposed refined approaches that incorporate the variability of the subgrade reaction coefficient along the length of the structure, thereby providing a more adequate representation of real foundation behavior.

The advancement of scientific thought has led to the development of more sophisticated models that incorporate variable stiffness characteristics, dissipative properties of the foundation, and the effects of non-stationary or moving loads. Among the effective numerical approaches for modeling the stress-strain state of beams on elastic foundations with variable parameters is the nodal acceleration method [8]. This method combines high computational accuracy with efficiency in resource utilization. The current stage of research is characterized by a transition from simplified analytical schemes to highly detailed numerical-analytical models, which enable the solution of applied problems in transportation and civil infrastructure.

In engineering practice, composite beams with intermediate hinges are frequently encountered, and the compliance of these hinges has a significant effect on the stress-strain state of the structure. The problem of accounting for elastic intermediate hinges has long remained insufficiently investigated, despite its practical relevance for designing structures under variable stiffness and consolidation conditions. An improved mathematical model was proposed in [9], [10] based on the introduction of corrective terms into the differential equation of beam bending to account for hinge compliance. To describe angular displacements at the interfaces between beam segments, the delta-function method and the Heaviside function are employed, which enables the incorporation of local effects into the computational model.

The contact layer method has proven to be an effective tool for accounting for adhesive interactions between the layers of multilayer beams. This method is based on representing the contact layer as a transversely anisotropic medium composed of short, non-interconnected elastic rods. Such a formulation avoids inaccuracies inherent in classical models, such as the occurrence of infinite shear stresses at interlayer boundaries. An improved technique, combining the finite element method with the contact layer method, extends the scope of application and enables the modeling of layered beams in MATLAB, taking into account transverse shear deformations and variable boundary conditions of the layers. These methods provide higher modeling accuracy and enables assessment of the influence of contact stiffness and shear deformations on the stress-strain state of the structure [11], [12].

In [13], a simplified finite element model was presented for analyzing a beam on a two-parameter elastic foundation. The model incorporates foundation characteristics (stiffness and shear resistance), formulates stiffness and reaction force matrices, and performs numerical calculations under various boundary conditions to validate its applicability. The results were compared with those of the well-known models by Winkler and Vlasov, confirming the applicability of the proposed approach in engineering practice. Contemporary research is focused on developing universal models capable of accounting not only for vertical but also for shear stresses, multilayer beam configurations, and variable stiffness of intermediate layers. This research direction is particularly relevant for the analysis of composite structures, where different materials jointly sustain complex loading conditions. Increasing attention has been given to the use of numerical methods, including the finite element method, which enables the incorporation of complex geometries, boundary conditions, and nonlinear effects such as plasticity, cracking, and creep in materials [14], [15]. Models considering geometric and physical nonlinearities are crucial for stress analysis under real operating conditions. Advances in finite and boundary element methods, as well as variational approaches, have improved the accuracy of modeling structures on deformable foundations. Recent studies emphasize achieving both analytical interpretability and computational efficiency, while also ensuring experimental verification to enhance practical applicability in engineering [16], [17].

The relevance of this research arises from the identified research gap associated with the limitations of classical models for analyzing structures on elastic foundations. In particular, Winkler's model, which represents the foundation as a system of independent elastic elements, fails to capture the actual stress-strain state of the soil. Vlasov's model, although extending the formulation of the problem, also introduces simplifications, notably neglecting lateral interactions that significantly affect structural behavior. The absence of a comprehensive model in existing publications justifies the need for further research. The identified research gap demonstrates that there is still no comprehensive model that adequately captures both normal and shear stresses in beams on elastic foundations while maintaining computational efficiency. Therefore, the aim of this study is to develop an advanced mathematical model of a two-parameter elastic foundation, which eliminates the limitations of existing approaches, provides a more accurate description of the stress-strain state, and enhances the reliability of engineering design.

2. Methods

Consider a straight elastic beam of length l and thickness h_0 composed of a homogeneous isotropic material with elasticity modulus E. The beam is defined in a Cartesian coordinate system as $\left(-\frac{l}{2} \leq x_1 \leq \frac{l}{2}, -\frac{h_0}{2} \leq x_3 \leq \frac{h_0}{2}\right)$. The foundation is modeled as a 2-parameter elastic medium of finite thickness h, with its material characterized by an effective modulus of elasticity $\bar{E}$ (Figure 1) [18].
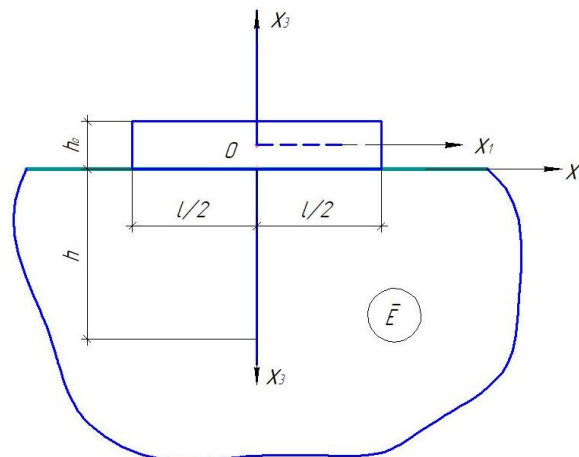

Figure 1 – Beam on a two-parameter elastic foundation

In the problem of beam-foundation interaction, where the foundation is modeled as a linearly deformable elastic half-plane, a key step is the correct formulation of the interface conditions between the structural elements. These conditions ensure the continuity of displacements and the consistency of the stress state at the beam-foundation interface. The coupling condition can be formulated as follows: the deflection of the beam must coincide with the deflection of the elastic foundation surface, i.e., $W_0(x_1) = W(x_1)$.

For the modeling of the elastic foundation in stress-strain analysis, the displacement function method is employed. Considering the effective modulus of elasticity $\bar{E}$ and the shear modulus G of the foundation material, the governing equilibrium equation can be expressed as follows:

$$\nabla^2 \nabla^2 F = \frac{\partial^4 F}{\partial x_1^4} + 2 \frac{\partial^4 F}{\partial x_1^2 \partial x_3^2} + \frac{\partial^4 F}{\partial x_3^4} = 0 \tag{1}$$

To solve the biharmonic Eq. (1), the displacement $F(x_1, x_3)$ is defined in the following form [19]:

$$F(x_1, x_3) = \delta(x_3) \cdot W(x_1), \tag{2}$$

where: $\delta(x_3)$ is the distribution function, and $W(x_1)$ is the foundation deflection function.

The governing Eq. (1), taking into account the transition relations $\frac{d^2 W(x_1)}{dx_1^2} = -\bar{k}^2 W(x_1)$, $\frac{d^4 W(x_1)}{dx_1^4} = \bar{k}_\omega^4 W(x_1)$ and the prescribed form of the displacement Eq. (2), can be written as follows:

$$\delta^{IV}(z_0) - 2 \cdot k^2 \delta''(z_0) + k_\omega^4 \delta(z_0) = 0 \tag{3}$$

The general solution of this equation is given by the expression $\lambda^2 = k^2(1 \pm \sqrt{1-\alpha})$; $k_\omega^4 = \alpha \cdot (k^2)^2$:

$$1.\ \alpha = 1:\ \delta(z_0) = (C_1 + C_2 z_0)e^{-kz_0} + (C_3 + C_4 z_0)e^{kz_0} \tag{4}$$

$$2.\ \alpha > 1:\ \delta(z_0) = [C_1 \cos(\beta_1 z_0) + C_2 \sin(\beta_1 z_0)]e^{-\alpha_1 z_0} + [C_3 \cos(\beta_1 z_0) + C_4 \sin(\beta_1 z_0)]e^{\alpha_1 z_0} \tag{5}$$

$$3.\ \alpha < 1:\ \delta(z_0) = C_1 e^{a_2 z_0} + C_2 e^{-a_2 z_0} + C_3 e^{\beta_2 z_0} + C_4 e^{-\beta_2 z_0}, \tag{6}$$

where: $\alpha_1 = k\sqrt{\frac{\alpha+1}{2}}$; $\beta_1 = k\sqrt{\frac{\alpha-1}{2}}$; $\alpha_2 = k\sqrt{1 - \sqrt{1-\alpha}}$; $\beta_2 = k\sqrt{1 + \sqrt{1-\alpha}}$.

The results obtained from Eq. (4) are discussed in detail in [19]. In the present study, the main focus is placed on the analysis of Eq. (5) and the derivation of the corresponding solutions. The general solution of Eq. (5) is applied to the problem of a semi-infinite elastic half-plane, which serves as the basis for the subsequent analysis ($z_0 \to \infty$, $\delta(z_0) = 0$):

$$\delta(z_0) = [C_1 \cos(\beta_1 z_0) + C_2 \sin(\beta_1 z_0)]e^{-\alpha_1 z_0} \tag{7}$$

When applying the displacement method, the unknown constants, parameters, and the governing equation included in the fundamental relations are determined as follows. The unknown constants:

$$C_1 = \frac{1}{12\alpha_p}[2v\alpha_1 \alpha \alpha_0 + (\alpha - v)\beta_0]$$

$$C_2 = -\frac{1}{12\beta_1 \alpha_p}[(\alpha + v)\alpha_1 \cdot \beta_0 - (1 + v)\alpha k^2 \alpha_0] \tag{8}$$

$$C_0 = \frac{1}{12}\frac{\bar{E}h^2}{Eh_0^2}\beta_0;\ A_0 = -\frac{1}{8} + \frac{1}{24}\frac{\bar{E}h^2}{Eh_0^2}\beta_0;\ B_0 = \frac{1}{24} - \frac{1}{32}\frac{\bar{E}h^2}{Eh_0^2}\beta_0 - \frac{1}{12}\frac{\bar{E}h^3}{Eh_0^3}\alpha_0$$

The parameters of the computational model are defined in terms of Poisson's ratio v, the stiffness characteristics of the foundation, and the relationships between its geometric dimensions and those of the beam. These parameters provide the basis for constructing the model and conducting further analytical investigations.

$$\alpha_0 = \frac{6(1-v)}{\alpha k^2(1+v)}\alpha_p P_1;\ \beta_0 = 12(1-v)\alpha_p P_0;$$

$$P_0 = \frac{1 - \alpha v + \alpha_1 \frac{h_0}{h}}{(1-\alpha v)n_1 k^2 - 2\alpha_1 m};\ P_1 = \frac{2m + n_1 k^2 \frac{h_0}{h}}{(1-\alpha v)n_1 k^2 - 2\alpha_1 m} \tag{9}$$

$$n_1 = \alpha^2(1-v) - \alpha v(1+v) + 2v; \quad m = 2\alpha\alpha_1(1+v) + \alpha_p(1-v)\frac{\bar{E}h}{Eh_0};$$

$$\alpha_p = \alpha^2 v + 2\alpha v + v^2\alpha + \alpha - v$$

Based on Eqs. (8) and (9), the governing equation is formulated, which defines the stress-strain state of a beam resting on an elastic foundation:

$$\gamma \cdot \frac{d^4 W_0(x_1)}{dx_1^4} = \frac{q(x_1)}{EJ}; \quad J = \frac{h_0^3}{12}; \quad \gamma = 1 - 6(1-v)\alpha_p \cdot P_0\frac{\bar{E}h^2}{Eh_0^2} - \frac{6(1-v)\alpha_p \cdot P_1}{\alpha k^2(1+v)}\frac{\bar{E}h^3}{Eh_0^3} \quad (10)$$

Taking into account the transition relations, the derived governing Eq. (10) can be reduced to the form of the standard beam-on-elastic-foundation equation, which has been widely applied in numerous theoretical and applied studies: $\frac{d^4 W_0(x_1)}{dx_1^4} - 2r^2\frac{d^2 W_0(x_1)}{dx_1^2} + S^4 \cdot W_0(x_1) = \frac{q(x_1)}{EJ}; \quad 2r^2 = -\frac{6(1-v)\alpha_p k^2 \cdot P_0}{h^2}\frac{\bar{E}h^2}{Eh_0^2}; \quad S^4 = -\frac{6(1-v)\alpha_p k^2 \cdot P_1}{(1+v)h^4}\frac{\bar{E}h^3}{Eh_0^3}.$

The bending moment M and the shear force Q of the beam are determined through integral relations that incorporate the normal and shear stresses along the section height. As a result, expressions are obtained that establish the relationship between these internal force factors and the deflection function W_0, the flexural rigidity EJ, as well as the foundation parameters g_1 and g_2, which are defined by integrals of the functions $\varphi_0(z)$ and $\psi_0(z)$ [20].

$$M = h_0^2 \int_{-\frac{1}{2}}^{\frac{1}{2}} \sigma_1^0 \cdot z\,dz = -EJ \cdot g_1 \cdot \frac{d^2 W_0(x_1)}{dx_1^2}$$

$$Q = h_0 \int_{-\frac{1}{2}}^{\frac{1}{2}} \tau_{13}^0 \cdot dz = EJ \cdot g_2 \cdot \frac{d^3 W_0(x_1)}{dx_1^3} \quad (11)$$

$$g_1 = 12 \int_{-1/2}^{1/2} \varphi_0(z) \cdot z\,dz, \quad g_2 = 12 \int_{-1/2}^{1/2} \psi_0(z)\,dz$$

The normal and shear stresses in the beam are defined through the internal forces according to Eq. (11). These relations establish a link between the stress state of the material and the integral parameters characterizing the section behavior, namely the bending moment and the shear force. This procedure enables a more detailed analysis of the stress distribution along the section height and accounts for the influence of the geometric and mechanical parameters of the beam on its stress-strain state [21].

$$\sigma_1^0 = h_0 \cdot \varphi_0(z)\frac{M}{J}$$

$$\tau_{13}^0 = -h_0^2 \cdot \psi_0(z)\frac{Q}{g_0 J} \quad (12)$$

$$\sigma_3^0 = h_0^3 \cdot \delta_0(z)\frac{q(x_1)}{\gamma \cdot J}$$

$$\psi_0(z) = A_0 - C_0 z + \frac{z^2}{2}$$

$$\delta_0(z) = B_0 - A_0 \cdot z + C_0\frac{z^2}{2} - \frac{z^3}{6},$$

where: $\psi_0(z)$ and $\delta_0(z)$ are the stress distribution functions.

The displacement components of the beam are obtained by integrating the expressions describing linear and transverse shear deformations [22]. This calculation scheme establishes an analytical relationship between the deflection function and the internal deformation parameters, thereby enabling a consistent consideration of shear effects in the development of the computational model.

$$U_3^0(x_1, x_3) = W_0(x_1)$$

$$U_1^0(x_1, x_3) = -h_0 \cdot \varphi_0(z)\frac{dW_0(x_1)}{dx_1} \quad (13)$$

$$\varphi_0(z) = -C_0 + z; \quad z = \frac{x_3}{h_0},$$

where: $\varphi_0(z)$ is the shear displacement distribution function (U_1^0); $W_0(x_1)$ is the beam deflection function (normal displacement); C_0 is an undetermined constant; z is the dimensionless transverse coordinate.

At the beam ends, one of the following boundary conditions must be satisfied [23]:

1) In the case where the beam end is in full contact with the elastic foundation:

$$W_* = \frac{Q \cdot L^3}{3\bar{E}J_0}; \quad \varphi_* = \frac{M \cdot L}{\bar{E}J_0}; \quad J_0 = \frac{h^3}{12}, \tag{14}$$

where: W_* and φ_* are vertical and angular displacements at the beam end; Q, M are the internal forces (shear force and bending moment, respectively) at the corresponding beam ends; L is the length of the deformable foundation; $\bar{E}J_0$ is the bending stiffness of the deformable foundation (h is its thickness; $\bar{E}$ is the elastic modulus of the foundation material);

2) In the case where a hinged support is installed at the beam end:

$$W_0 = 0; \quad M = -EJ\frac{d^2W_0(x_1)}{dx_1^2} = 0 \tag{15}$$

3) In the case where the beam end is rigidly clamped:

$$W_0 = 0; \quad \theta = \frac{dW_0(x_1)}{d(x_1)} = 0 \tag{16}$$

where: θ is the rotation angle.

4) In the case where the beam end is free (no contact) [23]:

$$M = -EJ\frac{d^2W_0(x_1)}{dx_1^2} = 0; \quad Q = -EJg_0\frac{d^3W_0(x_1)}{dx_1^3} = 0 \tag{17}$$

For a beam resting on a two-parameter elastic foundation, the construction of the analytical model requires consideration of the following fundamental parameters:

1) E, h_0, l, $q(x_1)$ – modulus of elasticity of the beam material, beam thickness (height), beam length, and the magnitude of the uniformly distributed load;

2) $\bar{E}$, ν, h, L – modulus of elasticity of the elastic foundation material, Poisson's ratio, thickness, and the extent of the region over which the beam's influence spreads beyond the contact zone.

To determine the stress-strain state of the beam-foundation interaction, the following sequence of computational steps is performed:

1) The governing Eq. (10) is solved subject to boundary conditions (14)-(17), yielding the beam deflection function $W_0(x_1)$;

2) Internal forces are computed according to Eq. (11);

3) Stress components $\sigma_1^0, \tau_{13}^0, \sigma_3^0$ are determined using Eq. (12).

3. Results and Discussion

Analytical solutions have been derived for various boundary conditions, loading types, and for cases involving variations in the geometric and physical-mechanical characteristics of both the beam and the foundation. To ensure the reliability of the analysis and enable a meaningful comparison of results, numerical simulations were carried out in the Mathcad environment, providing a basis for validating the analytical solutions. A beam resting on a two-parameter elastic foundation is considered. The applied load is assumed to be a uniformly distributed load of q=*1 kN/m*. The beam length is taken as *l=1 m* and the height is h_0=*0.25m*. The beam is characterized by an elastic modulus of *E=1·10¹⁰Pa*. The physical and geometry parameters of the elastic foundations were $\bar{E} = 1Pa$, $\nu = 0.25$ and $h = 1m$.

The results of the comparison between the classical and the proposed methods for analyzing a beam on an elastic foundation, including deflections, bending moments, and shear forces, are presented in Tables 1-3 and Figures 2-4. The analysis demonstrates that the values obtained using the proposed method are in good agreement with those derived from the Winkler model.

Table 1 – Vertical displacement values

Case	The length of the beam				
	0	0.25	0.5	0.75	1.0
y	0	0.000711904	0.000999157	0.000711904	0
Wp	0	0.00071119	0.00099816	0.00071119	0

Table 2 – Bending moment values

Case	The length of the beam				
	0	0.25	0.5	0.75	1.0
Mv	0	0.093673	0.124892	0.093673	0
Mp	0	0.09358	0.12477	0.09358	0

Table 3 – Shear force values

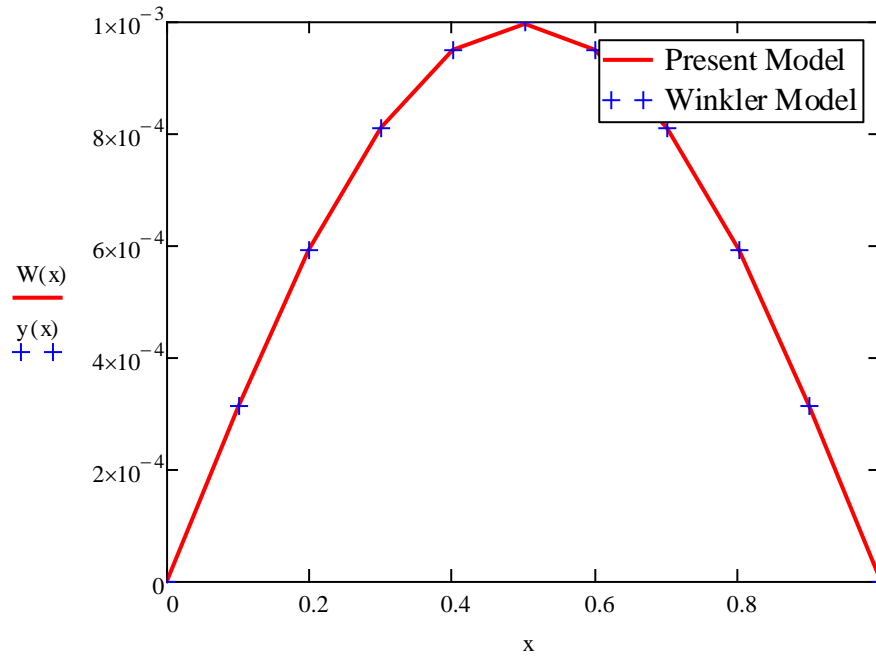| Case	The length of the beam				
	0	0.25	0.5	0.75	1.0
Qv	0.49966	0.24976	0	-0.24976	-0.49966
Qp	0.49892	0.24946	0	-0.24946	-0.49892

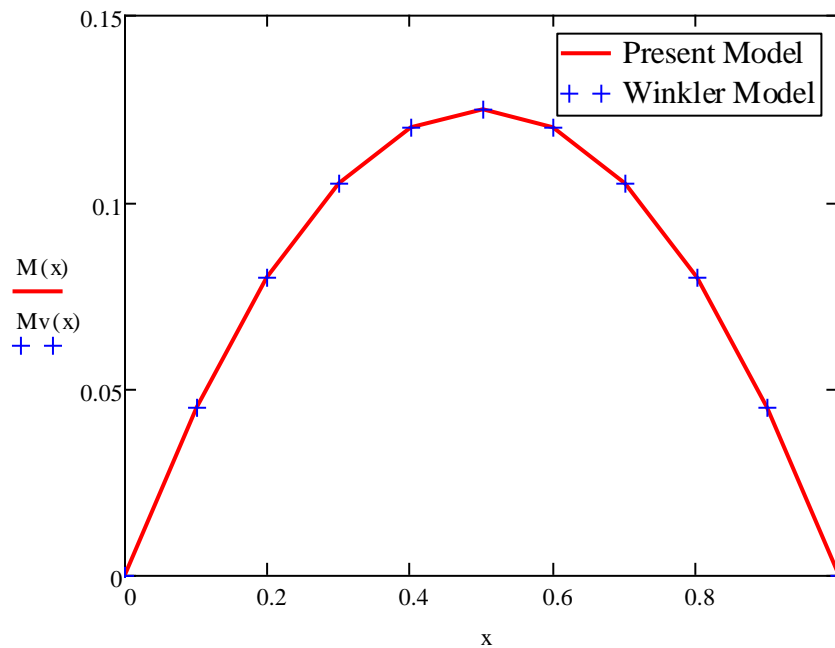Figure 2 – Vertical displacement of the beam on a two-parameter elastic foundation

Figure 3 – Bending moment of the beam on a two-parameter elastic foundation
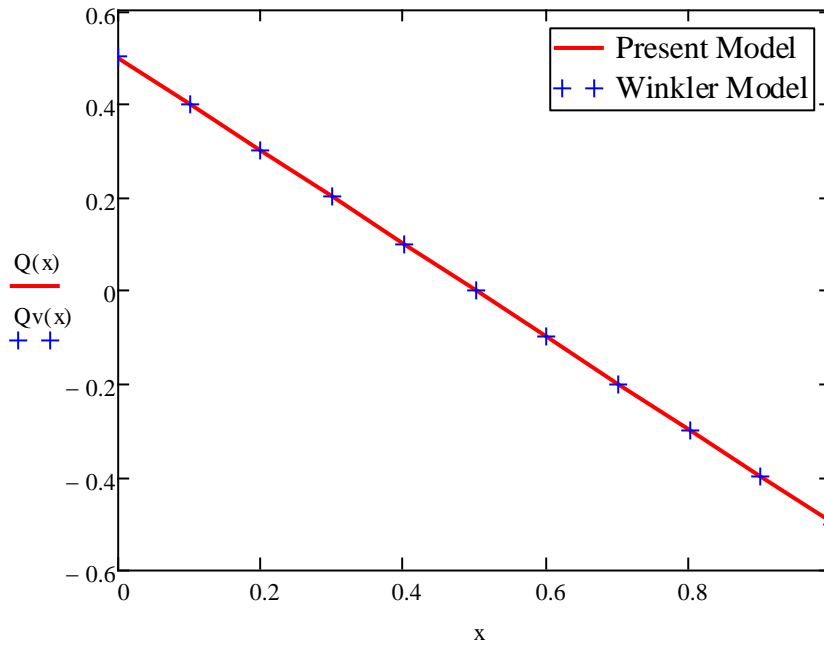
Figure 4 – Shear force of the beam on a two-parameter elastic foundation

The graphical results (Figures 2-4) for vertical displacement, bending moment, and shear force showed close agreement between the present study, the simplified formulation, and Winkler's classical solution. Tables 1, 2, and 3, as well as Figures 2, 3, and 4, present the calculation results for different beam lengths. As can be seen from the tables, the values obtained by the Present method showed good agreement with those calculated using the Winkler model. Maximum deflection was observed at the mid-span, while displacements decreased symmetrically toward the supports, and the distributions of bending moments and shear forces corresponded to theoretical expectations. The close coincidence of the curves confirmed the validity and reliability of the developed method, while the two-parameter model remained consistent with the Winkler approach and simultaneously provided broader applicability for more complex loading and heterogeneous foundation conditions.

Tables 4 and 5 present the values of shear and normal stresses calculated using the proposed method τ_{130}, σ_{10} and the Winkler model τ_{13v}, σ_{1v} at different points of the beam cross-section. The analysis shows that the maximum shear stresses are observed near the fixed end of the beam (x=0, z=0), gradually decrease to zero at midspan, and reach negative values at the opposite boundary (x=1, z=1). The normal stresses vary linearly along the cross-sectional height: from negative in the lower zone (z=−1/2) to positive in the upper zone (z=1/2), while their values are close to zero in the region of the neutral axis (z=0). The comparative analysis indicates a high degree of consistency between the results of the two methods, as evidenced by the nearly coincident values. Figure 5 shows the distribution of shear stresses along the beam cross-sectional height, while Figure 6 illustrates the distribution of normal stresses. In both cases, a high degree of agreement is observed between the results obtained by the proposed method and those of the classical Winkler model.

Table 4 – Shear stress results

Case	x=0, z=0	$x=\frac{1}{4}$, z=0	$x=\frac{1}{2}$, z=0	$x=\frac{3}{4}$, z=0	x=1, z=0
τ_{130}	2.995	-1,498	0	-1,498	-2,995
τ_{13v}	2.998	-1,499	0	-1,499	-2,998

Table 5 – Normal stress results

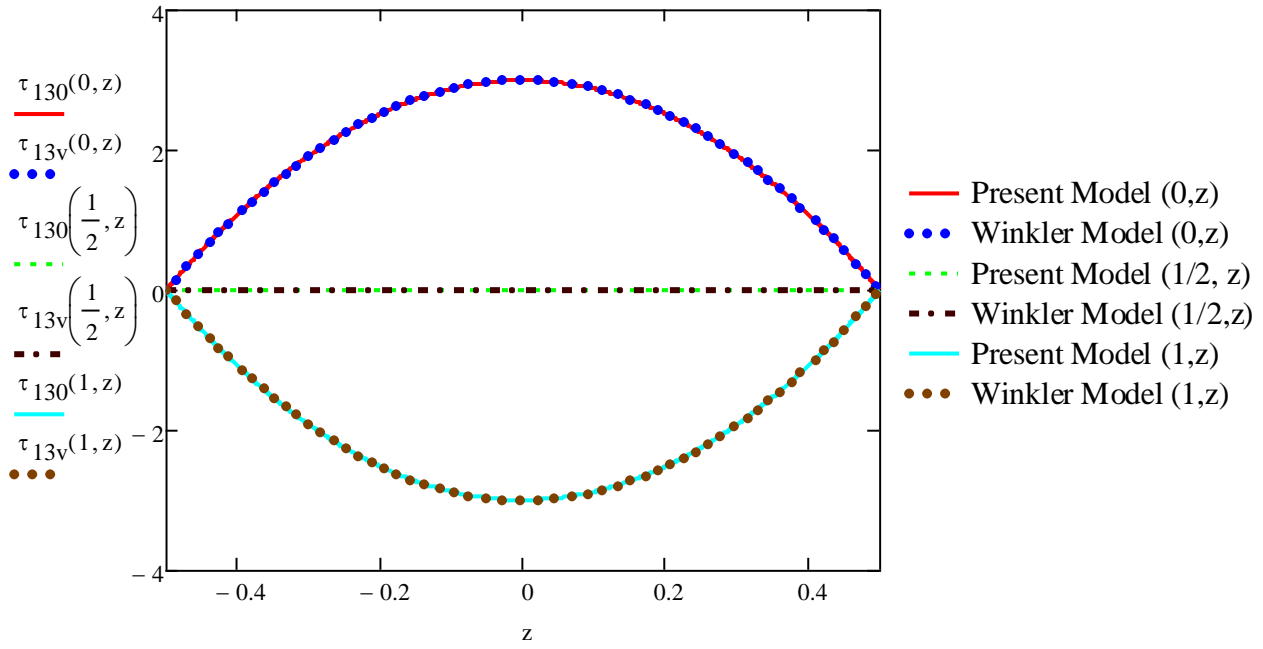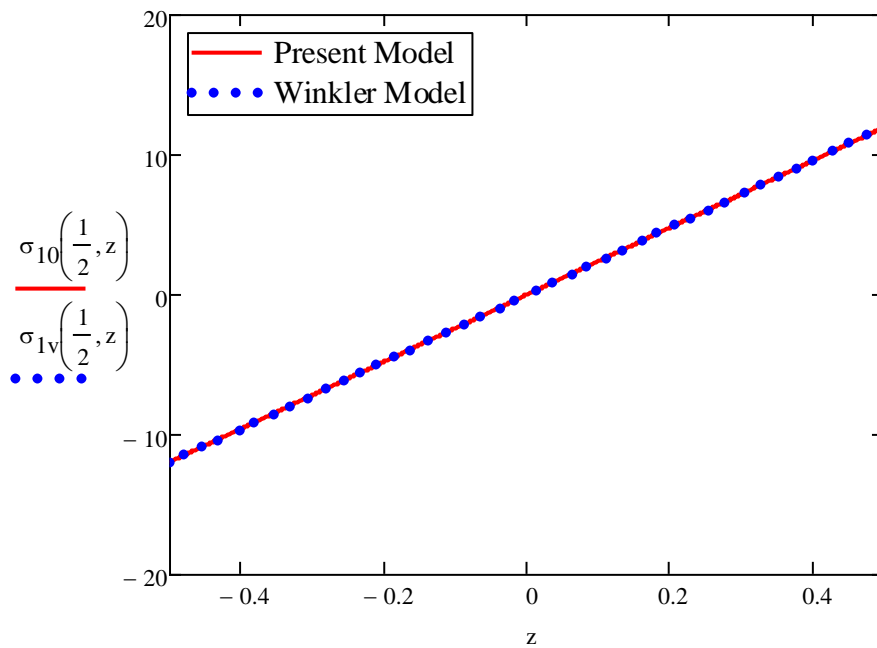| Case	$x=\frac{1}{2}$, $z=-\frac{1}{2}$	$x=\frac{1}{2}$, $z=-\frac{1}{4}$	$x=\frac{1}{2}$, z=0	$x=\frac{1}{2}$, $z=\frac{1}{4}$	$x=\frac{1}{2}$, $z=\frac{1}{2}$
σ_{10}	-11.977	-5.988	0.001217	5.988	11.977
σ_{1v}	-11.99	-5.995	0	5.995	11.99

Figure 5 – Distribution of shear stresses

Figure 6 – Normal stress distribution

Table 4 and Figure 5 present the shear stress values at the point $z = 0$ for varying coordinate x across five calculation points. As the results show, the values obtained using the proposed method are in good agreement with those calculated based on the Winkler model. Table 5 and Figure 6 provide the normal stress values at a constant x with varying coordinate z. These results also demonstrate consistency with the Winkler model, thereby confirming the validity of the proposed method. The comparative analysis demonstrated a high degree of consistency between the calculated stresses, confirming the reliability and applicability of the considered methods in engineering practice. The obtained findings not only enhanced the understanding of beam behavior on elastic foundations but also provided a basis for developing practical recommendations aimed at improving the accuracy and reliability of structural design.

4. Conclusions

An analytical solution has been developed for the stress analysis of beams resting on a two-parameter elastic foundation. The proposed mathematical model accounts for both normal and shear stresses, as well as the influence of the elastic foundation, enabling calculations for various boundary conditions and loading scenarios. The accuracy of the method has been verified through analytical examples and numerical simulations, including comparisons of vertical displacements, bending moments, and shear forces. Comparative evaluation with the classical Winkler model shows good agreement for vertical displacements, bending moments, and shear forces, while the proposed method provides improved accuracy in predicting both shear and normal stress distributions. The results confirm that the refined approach is reliable, practically applicable, and capable of capturing detailed stress-strain behavior that classical models may overlook. Overall, the developed simplified theory of a beam on a two-parameter elastic foundation is of significant interest to structural engineers involved in foundation design. It not only aligns well with classical Winkler predictions but also enhances the precision of stress analysis, providing a robust basis for practical applications and serving as a foundation for further research in structural mechanics and geotechnics.

References

[1] W. Sun and Z. Zhang, "Fourier series (based) multiscale method for computational analysis in science and engineering: VII. Fourier series multiscale solution for elastic bending of beams on Pasternak foundations," p. 32, Jan. 2023.

[2] M. Keikhaie, N. Keikhaie, R. Keikhaie, and M. M. Kaykha, "Stress Intensity Factors in Two Bonded Elastic Layers Containing Crack Perpendicular on the Interface with Different Elastic Properties," *Journal of Modern Physics*, vol. 06, no. 05, pp. 640–647, 2015, doi: 10.4236/jmp.2015.65070.

[3] V. Travush, V. Gordom, V. Kolchunov, and Y. Leontiev, "MATHEMATIC MODEL OF A BEAM PARTIALLY SUPPORTED ON ELASTIC FOUNDATION," *International Journal for Computational Civil and Structural Engineering*, vol. 15, no. 2, pp. 144–158, Jun. 2019, doi: 10.22337/2587-9618-2019-15-2-144-158.

[4] M. R. Miller, E. Y. Titov, S. S. Kharitonov, and Y. Fang, "The Stress-Strain State of the Tunnel Lining That Crosses the Fault Zone of Soil Blocks during an Earthquake," *Communications - Scientific letters of the University of Zilina*, vol. 24, no. 1, pp. D9–D22, Jan. 2022, doi: 10.26552/com.C.2022.1.D9-D22.

[5] N. V. Grigorevskiy, A. V. Zemskov, and A. V. Malashkin, "Modeling the Elastic-Diffusion Vibrations of a Hinged Timoshenko Plate under the Action of a Distributed Surface Load," *Mathematical Models and Computer Simulations*, vol. 15, no. S1, pp. S96–S110, Dec. 2023, doi: 10.1134/S2070048223070050.

[6] N. Challamel and I. Elishakoff, "A brief history of first-order shear-deformable beam and plate models," *Mech Res Commun*, vol. 102, p. 103389, Dec. 2019, doi: 10.1016/j.mechrescom.2019.06.005.

[7] C. Mittelstedt, *Buckling of Beams, Plates and Shells*. Berlin, Heidelberg: Springer Berlin Heidelberg, 2024. doi: 10.1007/978-3-662-69096-3.

[8] N. T. Phuoc and P. D. Trung, "The influence of mass of two-parameter elastic foundation on dynamic responses of beams subjected to a moving mass," *KSCE Journal of Civil Engineering*, vol. 20, no. 7, pp. 2842–2848, Nov. 2016, doi: 10.1007/s12205-016-0167-4.

[9] A. N. Beskopylny, E. E. Kadomtseva, G. P. Strelnikov, and Y. A. Berdnik, "Stress-strain state of reinforced bimodulus beam on an elastic foundation," *IOP Conf Ser Earth Environ Sci*, vol. 90, p. 012064, Oct. 2017, doi: 10.1088/1755-1315/90/1/012064.

[10] Z. Li, Y. Xu, and D. Huang, "Accurate solution for functionally graded beams with arbitrarily varying thicknesses resting on a two-parameter elastic foundation," *Journal of Strain Analysis for Engineering Design*, vol. 55, no. 7–8, 2020, doi: 10.1177/0309324720922739.

[11] V. I. Andreev, R. A. Turusov, and N. Y. Tsybin, "Determination of stress-strain state of a three-layer beam with application of contact layer method," *Vestnik MGSU*, no. 4, pp. 17–26, Apr. 2016, doi: 10.22227/1997-0935.2016.4.17-26.

[12] M. Skrinar, M. Uranjek, I. Peruš, and D. Imamović, "A New Beam Finite Element for Static Bending Analysis of Slender Transversely Cracked Beams on Two-Parametric Soils," *Applied Sciences*, vol. 11, no. 22, p. 10939, Nov. 2021, doi: 10.3390/app112210939.

[13] S. B. Akhazhanov, N. I. Vatin, S. Akhmediyev, T. Akhazhanov, O. Khabidolda, and A. Nurgoziyeva, "Beam on a two-parameter elastic foundation: simplified finite element model," *Magazine of Civil Engineering*, vol. 121, no. 5, 2023, doi: 10.34910/MCE.121.7.

[14] N. Kopiika, A. Klym, Y. Blikharskyy, D. Katunský, V. Popovych, and Z. Blikharskyy, "Evaluation of the stress-strain state of the RC beam with the use of DIC," *Production Engineering Archives*, vol. 30, no. 4, pp. 463–476, Dec. 2024, doi: 10.30657/pea.2024.30.44.

[15] E. Öztekin, "Theoretical analysis of stress-strain behavior of multi-layer RC beams under flexure," *Structural Engineering and Mechanics*, vol. 90, no. 5, pp. 505–515, 2024, doi: 10.12989/sem.2024.90.5.505.

[16] T. Qing-lin, Zh. Yi, G. Yong-ying, and N. Ben, "Stress-strain relationship analysis of pvc-frp confined steel reinforced concrete columns under axial compressive," *Engineering Mechanics*, vol. 2, 2025.

[17] K. Liu, J. Liang, C. Wang, X. Wang, and J. Liu, "Axial compression stress-strain relationship of lithium slag rubber concrete," *Sci Rep*, vol. 14, no. 1, p. 23037, Oct. 2024, doi: 10.1038/s41598-024-73566-7.

[18] S. Akhazhanov, "Serpimdili negizdegi arkalykty esepteu adisi," Karaganda: Karaganda State University named after E.A. Buketov, 2020, p. 166.

[19] S. Akhazhanov, D. Baltabai, and B. Nurlanova, "Refined mechanical and mathematical model of an elastic half-plane," *Technobius*, vol. 2, no. 1, p. 0014, Mar. 2022, doi: 10.54355/tbus/2.1.2022.0014.

[20] V. Struzhanov and N. Burmasheva, "Teoriya uprugosti: osnovnye polozheniya," Yekaterinburg: Ural University Publishing, 2019, p. 204.

[21] Y. Chen, C. Li, S. Wang, Y. Wang, and D. Li, "Theoretical Solution of Elastic Foundation Beam based on the Principle of Minimum Complementary Energy," *Journal of Engineering Science and Technology Review*, vol. 14, no. 3, pp. 51–58, 2021, doi: 10.25103/jestr.143.06.

[22] S. Akhazhanov, B. Bostanov, A. Kaliyev, T. Akhazhanov, and A. Mergenbekova, "Simplified method of calculating a beam on a two-parameter elastic foundation," *International Journal of GEOMATE*, vol. 25, no. 111, Nov. 2023, doi: 10.21660/2023.111.3898.

[23] F. Yue, "A Refined Model for Analysis of Beams on Two-Parameter Foundations by Iterative Method," *Math Probl Eng*, vol. 2021, pp. 1–11, Apr. 2021, doi: 10.1155/2021/5562212.

Information about authors:
Sungat Akhazhanov – PhD, Associate Professor, Research Laboratory Applied Mechanics and Robotics, Karaganda Buketov University, Karaganda, Kazakhstan, stjg@mail.ru
Nikolai Vatin – Dr.Sci.Eng., Professor, Scientific and Technological Complex "Digital engineering in civil construction", Peter the Great St. Petersburg Polytechnic University, St. Petersburg, Russia, vatin@mail.ru
Abai Kasimov – Candidate of Technical Sciences, Associate Professor, Department of Building Materials and Technologies, Abylkas Saginov Karaganda Technical University, Karaganda, Kazakhstan, kasimov3115@mail.ru
Aigerim Kassenova – PhD Student, Department of Building Materials and Technologies, Abylkas Saginov Karaganda Technical University, Karaganda, Kazakhstan, kasenova.aigerim@mail.ru

Author Contributions:
Sungat Akhazhanov – drafting, methodology, modeling.
Nikolai Vatin – editing, concept.
Abai Kasimov – data collection, analysis.
Aigerim Kassenova – visualization, data collection.

Conflict of Interest: The authors declare no conflict of interest.

Use of Artificial Intelligence (AI): The authors declare that AI was not used.